

2 *Article*

3
4 Modeling Smoke Plume-Rise and Dispersion from Southern United States Prescribed
5 Burns with Daysmoke

6
7 **Gary L. Achtemeier^{1*}, Scott A. Goodrick¹, Yongqiang Liu¹, Fernando Garcia-**
8 **Menendez², Yongtao Hu², M. Talat Odman²**

9
10 ¹ Center for Forest Disturbance Science, USDA Forest Service, Athens, GA30602, USA;

11 ² School of Civil and Environmental Engineering, Georgia Institute of Technology,
12 Atlanta, GA 30332-0512, USA.

13
14 E-Mails: sgoodrick@fs.fed.us, yliu@fs.fed.us, fernando@gatech.edu,
15 yh29@mail.gatech.edu, odman@gatech.edu.

16
17 Author to whom correspondence should be address; E-Mail: gachtemeier@fs.fed.us

18
19
20 **Abstract.** We present Daysmoke, an empirical-statistical plume rise and dispersion
21 model for simulating smoke from prescribed burns. Prescribed fires are characterized by
22 complex plume structure including multiple-core updrafts which makes modeling with
23 simple plume models difficult. Daysmoke accounts for plume structure in a three-
24 dimensional veering/sheering atmospheric environment, multiple-core updrafts, and
25 detrainment of particulate matter. The number of empirical coefficients appearing in the
26 model theory is reduced through a sensitivity analysis with the Fourier Amplitude
27 Sensitivity Test (FAST). Daysmoke simulations for “bent-over” plumes compare closely
28 with Briggs theory although the two-thirds law is not explicit in Daysmoke. However, the
29 solutions for the “highly-tilted” plume characterized by weak buoyancy, low initial
30 vertical velocity, and large initial plume diameter depart considerably from Briggs
31 theory. Results from a study of weak plumes from prescribed burns at Fort Benning GA
32 showed simulated ground-level PM_{2.5} comparing favorably with observations taken
33 within the first eight kilometers of eleven prescribed burns. Daysmoke placed plume tops
34 near the lower end of the range of observed plume tops for six prescribed burns.
35 Daysmoke provides the levels and amounts of smoke injected into regional scale air
36 quality models. Results from CMAQ with and without an adaptive grid are presented.

37
38 **Author Keywords:** smoke, prescribed fires, plume model, air quality

39 40 **1. Introduction**

41
42 The forests of the southern United States (the 13 States roughly south of the Ohio
43 River and from Texas to the Atlantic Coast) comprise one of the most productive forested
44 areas in the United States. Approximately 200 million acres (80 million ha) or 40% of
45 U.S. forests are found within this area - comprising only 24% of the U.S. land area [1].
46 These forests are dynamic ecosystems characterized by rapid growth within a favorable
47 climate. The fire-return interval of every 3-5 years is the highest in the nation [2].

48 Approximately six million acres (2.4 million ha) of forest and agricultural land are
49 burned each year in the southern United States to accomplish a number of land
50 management objectives [3](Wade et al. 2000). Smoke from these burns poses a threat –
51 either as a nuisance, visibility, or transportation hazard [4] [5], and/or as a health hazard
52 [6]. The hazard can be local and/or regional depending on the number of prescribed burns
53 being conducted on a given day.

54 Fires have been found to be an important source of $PM_{2.5}$ (particulate matter with
55 aerodynamic diameter of equal to or less than 2.5 micrometers) [7](Zheng et al. 2002).
56 Forestry smoke in the southern United States contributes significantly to the budget of
57 particulate matter in the atmosphere and efforts have been undertaken to include the
58 smoke in regional air quality models [8] [9] [10] [11] and [12]. Recent studies suggest
59 that prescribed burning alone may be contributing up to 30% of the annual $PM_{2.5}$ mass in
60 the Southeastern United States [13] and may be the leading cause of high $PM_{2.5}$ episodes
61 in the region [14]. For example, the simulation studies of a number of prescribed burns in
62 the Southern U.S. with the Community Multiscale Air Quality model (CMAQ, [15] and
63 [16]) indicated that smoke plumes caused severe air quality problems in downwind
64 metropolitan areas with the ground $PM_{2.5}$ concentrations much higher than the daily (24-
65 h) US National Ambient Air Quality Standard.

66 Regional scale air quality models require knowledge of how much smoke is
67 discharged into the atmosphere as the plume rises to some maximum height. Plume rise
68 ranges from hundreds of meters for prescribed fires to thousands of meters for wildfires.
69 However, plume rise and dispersion from wildland fires is difficult to model because of
70 complex plume dynamics. For example, Figure 1 shows the GOES satellite image of the
71 plume produced by the 27 February 2004 Magazine Mountain, AR, prescribed burn (red
72 area) at 2045 UTC. The image, showing an expanding single plume transported towards
73 northwestern Arkansas by the prevailing wind, gives an impression of being from a
74 “scaled-up” version of an industrial plume. However, Figure 2 reveals a complex
75 structure of merging multiple updraft “cores” when the plume is viewed from the ground.

76

77 Figure 1. 2115 UTC GOES image of the smoke plume from the 27 February 2004
78 Magazine Mountain, AR, prescribed burn (red area).



79

80

81 Clearly the updraft structure of wildland fire plumes must be modeled correctly if
 82 accurate estimates for plume rise, amounts and heights of smoke injection in the
 83 atmosphere, and dispersion are to be made available for air quality models. Full-physics
 84 smoke plume models such as the active tracer high-resolution atmospheric model
 85 (ATHAM) [17] [18] can model the complexity of wildland fire plume structures. [19]
 86 simulated a prescribed burn in northwestern Washington which closely approximated
 87 measured elevations and concentrations of smoke. However, if the objective is to
 88 simulate hundreds of prescribed burns daily in the southern United States, much simpler
 89 modeling approaches would be required to make available plume rise data for operational
 90 air quality models such as CMAQ [16], its adaptive grid version [20] or WRF-Chem [21]
 91 for predicting air quality and assessing pollution control strategy development, exposure,
 92 impacts of regional climate change, and etc.

93
 94 Figure 2. Photo-images of the smoke plume above the 27 February 2004 Magazine
 95 Mountain, AR, prescribed burn.



96
 97
 98 [22] linked fuels information with meteorological data through VSMOKE, a
 99 Gaussian “screening” model for local smoke dispersion. VSMOKE attempted to account
 100 for plume complexity by placing 40% of smoke at the ground as an initial step. The
 101 Florida Fire Management Information System [23] [24] merges the cross flow Gaussian
 102 horizontal dispersion properties of VSMOKE with three dimensional trajectories
 103 produced by HYSPLIT [25] to estimate smoke plume movement and the ground-level
 104 impact of $PM_{2.5}$ concentrations on potentially hazardous visibility reductions.

105 This paper describes “Daysmoke,” an empirical-stochastic plume model designed to
 106 simulate multiple-core updraft smoke plumes from prescribed burns. Daysmoke is an
 107 extension of ASHFALL, a plume model developed to simulate deposition of ash from
 108 sugar cane fires [26]. As adapted for prescribed fire, Daysmoke consists of three models
 109 – an entraining turret model that calculates plume pathways, a particle trajectory model
 110 that simulates smoke transport through the plume pathways, and a meteorological
 111 “interface” model that links these models to weather data from high-resolution numerical

112 weather models.

113 Model theory and assumptions are described in the next section. Results from
114 validation studies for simulating weak plumes and applications to regional scale air
115 quality modeling follow.

116

117 **2. Model Theory and Description**

118

119 Conceptually, a rising convective plume driven by heat from combustion entrains
120 ambient air which adds to the plume mass while modulating its buoyancy and vertical
121 velocity. Some plume air and particulate matter are detrained into the ambient air creating
122 a “pall” of smoke extending downwind beneath the visible plume. The growing smoke
123 plume ascends to near the top of the mixing layer. If the smoke plume is relatively weak
124 (cool and slow-rising), all or part of it may be captured, torn apart, and dispersed by
125 turbulence within the mixed layer before it rises to an altitude of thermal equilibrium. If
126 the convective smoke plume is strong, most of the smoke may be ejected into the free
127 atmosphere far above the top of the mixed layer with little or no smoke remaining to be
128 dispersed within the mixed layer.

129

130 *The Entraining Turret Model*

131

132 From photogrammetric analysis of video footage of smoke plumes from burning
133 sugar cane, [27] determined that a rising smoke plume could be described by a train of
134 rising turrets of heated air that sweep out a three-dimensional volume defined by plume
135 boundaries on expanding through entrainment of surrounding air through the sides and
136 bottoms as they ascend (Figure 3). The change in the volume (V) of radius (r) and height
137 (h) of a rising turret by entrainment of ambient air as it passes from height $z-1$ to z is,

138

$$V_z = V_{z-1} + \Delta V$$

139

$$\text{where} \tag{1}$$

$$\Delta V = \pi(r + \Delta r)^2(h + \Delta h) - \pi r^2 h$$

140

141 and is distributed over three parts: (1) an annulus around the original cylinder, (2) a
142 cylinder added to the bottom of the original cylinder, and (3) an annulus around the added
143 cylinder as shown by the inset in Figure 3.

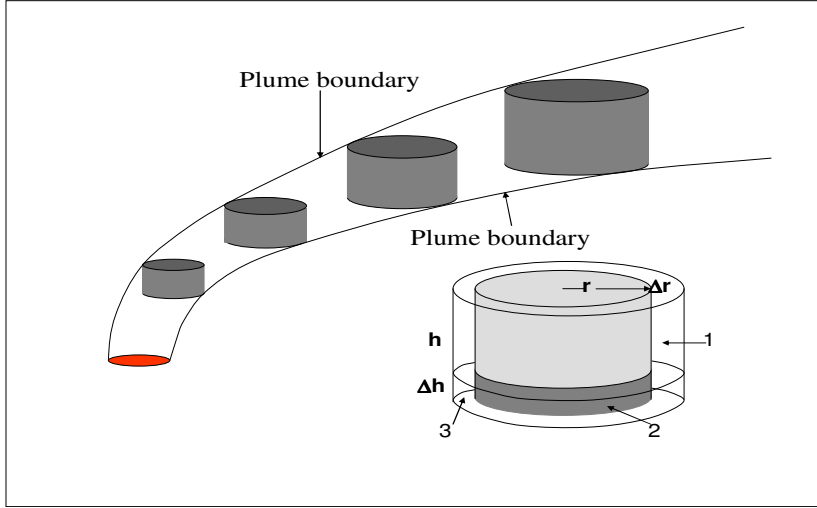
144

145 Entrainment of heat and momentum (horizontal and vertical) is a function of the
146 downwind tilt of the plume. For example, if the horizontal wind speed is zero (the plume
147 rises vertically), all of the material entrained through the bottom and top of the turret is
148 plume air while entrainment of ambient air takes place through the sides. As the plume
149 tilts in the presence of wind, more ambient air is entrained through the bottom and top of
150 the turret until, if the plume blows horizontally, all air entrained into the turret is ambient
151 air.

151

152

153 Figure 3. A schematic showing the boundaries of a smoke plume defined by rising,
 154 entraining turrets. Inset. three components of an expanding cylinder: (1) an annulus
 155 around the original cylinder, (2) a cylinder added to the original cylinder, and (3) an
 156 annulus around the added cylinder.



157

158

159 Let Q_e represent an ambient constituent, and Q_{z-1} represent the smoke plume
 160 constituent surrounding the turret at level $z-1$. The constituent Q_z at level z resulting from
 161 the mixing of the original turret with the entrained volume of mixed constituents is,
 162

163

$$Q_z V_z = Q_{z-1} V_{z-1} + Q' \Delta V \quad (2)$$

164

165 Where Q' is found by weighting annulus 1 by Q_e , weighting cylinder 2 by $a_1 Q_{z-1} + a_2 Q_e$,
 166 and weighting annulus 3 by $0.5(a_1 Q_{z-1} + a_2 Q_e + a_3 Q_e)$. This definition for Q' requires that
 167 all air entrained into annulus 1 carries the ambient constituent; air entrained into cylinder
 168 2 is a weighted sum of ambient and plume constituents; and air entrained into annulus 3
 169 is the average of the mixture entrained into cylinder 2 and the ambient constituent. The
 170 three constants are chosen so that $a_3 = a_1 + a_2 = 1$. Furthermore,
 171

172

$$a_2 = \frac{2}{\pi} A \tan \left| \frac{s}{w} \right|; (w \neq 0) \quad (3)$$

173

174 where s is the horizontal wind speed and w is the plume vertical velocity. From equation
 175 (3), if the horizontal wind is zero, the plume stands vertically, $a_2 = 0$, $a_1 = 1$, and
 176 entrainment from below is plume air. If the vertical velocity approaches zero, the plume
 177 drifts horizontally, $a_2 = 1$, $a_1 = 0$, and entrainment from below is ambient air. If $s = w$, the
 178 plume bends over to a 45 degree orientation, $a_2 = 0.5$, $a_1 = 0.5$, and entrainment is equally
 179 divided between ambient and plume air.

180

181 The derivation of the plume pathways is subject to two assumptions needed to
 182 make the problem tractable. First, changes in volume are equally distributed between
 183 deepening and expanding the turret. Second, the changes in volume will be functions of
 the rate of turret rise. Therefore,

184

$$185 \quad \Delta h = \Delta r = e w_{z-1} \Delta t \quad (4)$$

186

187 where e is an entrainment coefficient. This assumption is equivalent to the definition for
 188 entrainment in the early rising stages of bent-over plumes (Briggs, 1975). Inclusion of (4)
 189 into equations (1) and (2) gives a general algorithm for turret growth and for the
 190 evolution of constituents within the turret,

191

$$192 \quad Q_z V_z = Q_{z-1} V_{z-1} + \pi \left\{ \begin{aligned} &(e w_{z-1} \Delta t) [r^2 (a_1 Q_{z-1} + a_2 Q_e) + 2rhQ_e] + (e w_{z-1} \Delta t)^2 [2r(a_1 Q_{z-1} \\ &+ a_2 Q_e + Q_e) / 2 + hQ_e] + (e w_{z-1} \Delta t)^3 (a_1 Q_{z-1} + a_2 Q_e + Q_e) / 2 \end{aligned} \right\} \quad (5)$$

193

194 Setting $Q = T$ (temperature) in (5) yields an equation for turret temperature for buoyancy
 195 calculations. Setting $Q = (u, v, w)$ (any of the velocity components) yields an equation for
 196 plume drift. Setting $Q = 1$ yields an equation for the volume growth of the turret.

197

198 Initial conditions for plume temperature, rise rate, and volume start the plume
 199 rising through a veering/shearing horizontal wind field within a stratified atmosphere.
 200 Once the initial conditions are specified, Equation (5) is solved numerically to yield the
 201 plume pathway (Figure 3). In addition, the rise rate is adjusted for buoyancy through

201

$$202 \quad w_z = w_{z-1} + g \frac{T_z - T_e}{T_e} \left(\frac{\Delta z}{w_{z-1}} \right) \quad (6)$$

203

204 where g is the acceleration of gravity and T_e is the ambient temperature.

205

206 Equation (5) does not include adiabatic expansion of the rising plume. For the
 207 vast majority of prescribed burns in the southeastern United States (for which plume tops
 208 are less than 2 km), scale analysis shows that omission of adiabatic expansion leads to
 209 errors in the calculation of plume expansion of less than 3% - an error far smaller than
 210 uncertainties in the measurement of fuel characteristics. However, should Daysmoke be
 211 used in modeling of large plumes from wildfires, the errors of omission of adiabatic
 212 expansion can become significant – perhaps as large as 30% for plumes growing above
 213 10 km. Therefore adiabatic expansion is calculated from [28]

213

$$214 \quad d(\ln V) = -2.48d(\ln T) \quad (7)$$

215

216 where the change in T is the adiabatic temperature decrease the plume encounters on
 217 rising through a depth Δz .

218

219 Moist processes activate a simple cloud parameterization in Daysmoke. A
 220 cumulus cloud forms when the moisture (mixing ratio) within a rising, entraining turret
 221 exceeds the saturation mixing ratio calculated for the turret temperature. Both turret
 222 temperature and mixing ratio are calculated via Equation (5). The entire turret is assumed
 223 to be saturated. All liquid water remains within the cloud. The cloud ascends by a
 224 weighted average of the dry and moist adiabatic lapse rates calculated for the rising turret
 225 at its temperature and pressure. The cloud top is the elevation where the cloud mixing
 ratio falls below the saturation mixing ratio at plume temperature and pressure. Though

226 adequate for shallow cumulus clouds that may form over prescribed burn plumes, the
 227 cloud parameterization is not adequate for modeling deep, precipitating pyro-cumuli that
 228 form on occasion above intense wildfires.

229 In addition to ambient weather data, Equation (5) must be supplied with the
 230 entrainment coefficient (e) and initial values for the plume - effective plume diameter (D_0
 231 $= 2r_0$), vertical velocity (w_0), and the difference between plume and ambient temperatures
 232 (ΔT_0). The effective plume diameter is defined as the diameter a plume would have if
 233 emissions from an irregular-shaped burning area were spread over a circular area.

234 Observations of plumes from large-perimeter prescribed fires reveal the presence
 235 of several updraft cores or subplumes. These updraft cores may vary in size depending on
 236 the type, loading, and distribution of various fuels. Multiple-core updraft plumes, being
 237 smaller in diameter than a single core updraft plume, would be more impacted by
 238 entrainment and thus would be expected to grow to lower altitudes. If the effective plume
 239 diameter and initial vertical velocity are replaced by initial volume flux,
 240

$$241 \quad f_0 = \frac{\pi}{4} D_0^2 w_0 \quad (8)$$

242 then the volume fluxes of the individual updraft cores may be defined subject to the
 243 constraint that
 244

$$245 \quad f_k = f_0 \frac{(0.01 + ran_k)}{\sum_{k=1}^n (0.01 + ran_k)} \quad (9)$$

247 where ran_k is a random number $0 < ran_k < 1$. The 0.01 is summed with the random number
 248 to render the updraft core diameter unequal to zero. Thus Daysmoke can be set to create
 249 simultaneous plume pathways for any number of updraft cores. The caveat is that n and
 250 f_k , $k = 1, \dots, n$ are unknown. The f_k are estimated through the random number ran ,
 251 however, no mechanism to determine n exists in Daysmoke. Equation (5) needs D_{0k}
 252 which must be calculated from each f_k . The effective plume diameter can be calculated
 253 from each updraft core volume flux by
 254

$$255 \quad D_{0k} = \left(\frac{4f_k}{\pi w_0} \right)^{1/2} \quad (10)$$

257 However, defining what constitutes updraft cores is complicated by the merging
 258 convective sub-plumes often observed with prescribed burns (Figure 2). Thus the
 259 multiple-core updraft capability of Daysmoke remains an oversimplification of complex
 260 plume structures from prescribed burns. It becomes convenient to assert that a particular
 261 plume “behaves as an n -core updraft plume” even though the number of observed updraft
 262 cores may differ from n .
 263

264 The entrainment coefficient is calculated internally in Daysmoke. For calm air
 265 and neutral stratification, [29] found entrainment coefficients for vertical plumes from
 266 industrial stacks to range from 0.080 for “jets” (high momentum plumes of low

267 buoyancy) to 0.155 for buoyant plumes. For bent-over plumes, Briggs reported
 268 entrainment coefficients in the range from 0.52 to 0.66. Thus, for the full range of
 269 buoyant plumes (from erect through bent-over), entrainment coefficients vary from 0.155
 270 to 0.66. Let the entrainment coefficient be proportional to a plume “bent-overness” index
 271 B_0 defined as

272

$$273 \quad B_0 = \frac{\Delta x}{\Delta y} = \frac{S}{w_0} = \frac{S}{D_{0k}} \frac{D_m}{S_m} = 10 \frac{S}{D_{0k}} \propto e_k \quad (11)$$

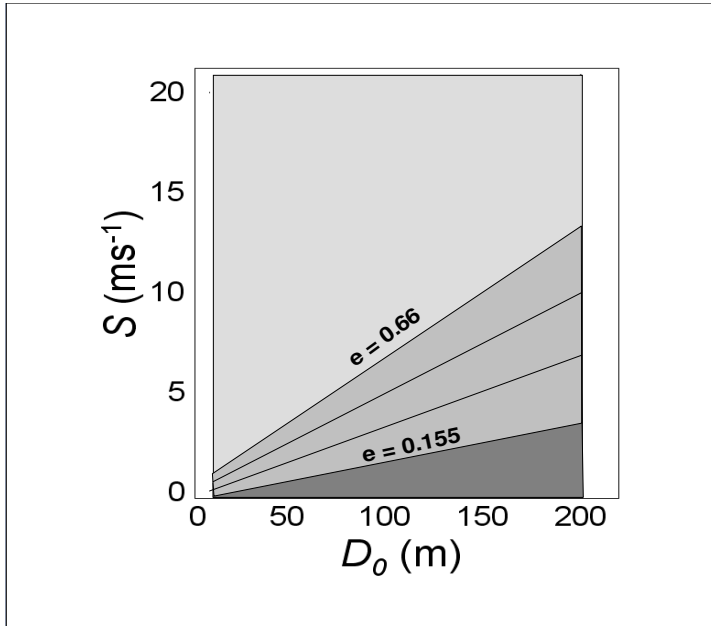
274

275 For prescribed burns, bent-overness can be represented as the ratio of the strength of the
 276 transport wind S with the strength of the plume as given by w_0 . However, w_0 is fixed in
 277 Daysmoke and the strength of the plume is better represented by the effective plume
 278 diameter D_0 . Let the ratio D_m/S_m represent a scaling factor determined by the range of S
 279 ($0 < S < 20 \text{ ms}^{-1}$) and of D ($0 < D < 200 \text{ m}$) for prescribed burns. The range of B_0 is
 280 subject to the constraint that $0.155 < e_k < 0.66$. Thus e_k becomes a dynamic variable that
 281 changes during the course of the day as the depth of the mixing layer and wind speeds
 282 change and during the course of the burn as plume conditions change.

283 Figure 4 maps entrainment coefficients for the ranges of transport wind speeds
 284 and initial plume diameters described above. Most of the area is assigned the maximum
 285 entrainment coefficient, $e_k = 0.66$ (light gray area) meaning most prescribed burns fit the
 286 bent-over designation. However, for larger diameter burns and/or weak to moderate
 287 transport wind speeds, the entrainment coefficient is variable within the range defined by
 288 the medium gray area.

289

290 Figure 4. Entrainment coefficient as a function of transport wind speed and initial plume
 291 diameter.



292

293

294

295

The Detraining Particle Model

296

297

298

299

300

301

302

303

304

305

306

Particles are released at the base of the multiple-core updraft plumes defined by the entraining turret module. Each particle represents a pre-assigned mass of smoke particulate matter. The particles ascend through each plume at the mean velocity components that define the three-dimensional wind speed for each level of the entraining turret module. The particles are spread laterally as the plume widens. At each time step there is added to these velocities a stochastic component that approximates turbulent spreading of smoke as it rises.

The location of a particle over an interval of time, Δt , as it traverses the plume volume is given by,

$$\begin{aligned} x^t &= x^{t-1} + [u + 2e(0.5 - \text{ran}_u)]\Delta t \\ y^t &= y^{t-1} + [v + 2e(0.5 - \text{ran}_v)]\Delta t \\ z^t &= z^{t-1} + [w + w_f + 2e(0.5 - \text{ran}_w)]\Delta t \end{aligned} \quad (12)$$

308

309

310

311

312

313

314

315

316

where the entrainment coefficient e in the stochastic term links particle spread with plume spread calculated in the entraining turret module. Here ran_k is a random number $0 < \text{ran}_k < 1$. The variable w_f is the fall speed (terminal velocity) of the particle. Each particle is tracked through the plume volume until it is discharged into the free atmosphere by either (1) detrainment across plume boundaries, (2) plume capture by convective circulations, or (3) discharge through the plume top when plume vertical velocity falls below a threshold vertical velocity w_c .

317

318

The Meteorological Interface Model

319

320

321

322

323

324

325

326

327

The interface model can be of any design and complexity but, for operational considerations, it has been kept relatively simple. The interface model links Daysmoke with hourly vertical profiles of weather data taken from numerical weather prediction models. These data are hourly averages and do not represent high frequency processes that mix and disperse smoke within the boundary layer. Therefore the interface model includes a simple formulation for deep convective mixing.

After a particle is discharged from the plume, the change in its position is given by,

$$\begin{aligned} x^t &= x^{t-1} + [u + u_s + u_{ce}]\Delta t \\ y^t &= y^{t-1} + [v + v_s + v_{ce}]\Delta t \\ z^t &= z^{t-1} + [(w_a + w_f) + w_s + w_{ce}]\Delta t \end{aligned} \quad (13)$$

329

330

331

332

333

where the velocity components (u, v) represents the steady part of the wind taken from the profiles of hourly weather data and subscripts s and ce represent small scale and convective mixing. In addition, w_a represents the hourly vertical velocity of the ambient air and w_f is the terminal velocity of the particle. Small scale mixing is stochastic.

334 However, unrealistic concentrations of particles can occur just below the mixing height
 335 where there exist steep gradients in mixing. Thus, in Daysmoke,
 336

$$\begin{aligned}
 337 \quad u_s &= c_s 2(0.5 - \text{ran}_u) \\
 v_s &= c_s 2(0.5 - \text{ran}_v) \\
 w_s &= 0
 \end{aligned}
 \tag{14}$$

338
 339 where r_x and r_y are random numbers and c_s is the small scale mixing coefficient.

340 The formulation for convective circulations is described in Appendix A. A string
 341 of two-dimensional mass conservative sinusoidal circulation cells oriented normal to the
 342 mean wind vector within the mixing layer and with a translation speed equal to the mean
 343 wind vector describe the convective boundary layer. The cells are mutually independent –
 344 amplitude, phase, wavelength and time history may differ. The equations in Appendix A
 345 yield the convective velocity components (u_{ce} , v_{ce} , w_{ce}) for each particle subject to
 346 knowledge of the reference rotor velocity, w_r (ms^{-1}), for a mixing layer depth of 1 km.
 347

348 **3. Model Analysis (FAST Analysis and Comparison with Briggs Theory)**

349 *a) FAST Analysis*

350
 351
 352 Table 1 lists coefficients, the range of values, the assigned values and the expected
 353 impacts on plume height (P. Hgt) and ground-level concentrations of particulate matter
 354 (GLC). The ranges of values have been determined through approximately 200
 355 simulations to define “reasonable” facsimiles of prescribed fire smoke plumes.
 356

357 Table 1. Assigned coefficients and constants and the expected impact on Daysmoke.

358 Constant	359 Definition	360 Range of Value	361 Assgn Value	362 Impact	
				P Hgt.	GLC
363 n (none)	updraft core number	1-10	user input	major	major
364 c_s (ms^{-1})	lateral plume spread	0.2-0.5	0.30	none	major
365 w_c (ms^{-1})	threshold velocity	0.1-1.0	0.35	none	none
366 w_f (ms^{-1})	particle terminal velocity	----	0.0002	none	none
367 w_r (ms^{-1})	max rotor velocity	0.5-2.0	1.0	none	major

368 The updraft core number n ranges between one and ten for prescribed burns
 369 typical of the southern United States. The updraft core number is specific to each burn
 370 and is critical for determining plume height and ground-level smoke concentration.

371 The small scale mixing coefficient c_s is the only mechanism in Daysmoke for the
 372 horizontal spread (normal to the plume axis) of the smoke plume. The simulations
 373 determined that the small scale mixing coefficient must fall in the range $0 < c_s < 1$. There
 374 was no lateral plume spread with $c_s = 0$. Simulations with $c_s = 1$ spread the plume too
 375 broadly with ground-level smoke concentrations too low as compared with observed
 376 concentrations. A more realistic range for c_s is $0.2 < c_s < 0.5$. Other factors of plume
 structure, such as the definition and persistence of convective eddies in vertical cross

377 sections of smoke plumes simulated by Daysmoke, support the choice of $c_s = 0.3$.

378 The threshold vertical velocity ranges between $0.1 < w_c < 1.0 \text{ ms}^{-1}$. It was found
 379 that vertical velocity profiles for strong plumes that penetrate into stable airmasses above
 380 the mixing height typically decline the final meter per second over a short distance –
 381 usually less than 20 m. Weak plumes that do not penetrate above the mixing height are
 382 broken up by turbulence and dispersed within the mixing layer. Thus the choice for w_c for
 383 either strong or weak plumes has little impact on plume height or ground-level smoke
 384 concentrations.

385 The detraining particle module does require specification for two variables:
 386 terminal velocity w_f and threshold vertical velocity w_c . In Daysmoke, the terminal
 387 velocity is $w_f = -0.0002 \text{ ms}^{-1}$. For the range of applications of Daysmoke, w_f is negligible
 388 and has no impact on model calculations nor smoke sedimentation.

389 The expected range for the reference rotor velocity for a mixing layer of depth 1
 390 km lies between $0.5 < w_r < 2.0 \text{ ms}^{-1}$. Choosing w_r too small reduces the rate smoke is
 391 transported from aloft to the ground thus yielding smoke concentrations that are too small
 392 relative to observations. Simulation results suggest $w_r = 1.0 \text{ ms}^{-1}$.

393 Given assigned values for the coefficients in Table 1, only the updraft core
 394 number remains to be determined. Factors contributing to updraft core number include:
 395 size of the burn, shape of burn area, heterogeneity of fuels, fuel type, moisture, and
 396 loadings, distribution of fire on landscape, amount of fire on landscape, distribution of
 397 canopy gaps, transport wind speed, and mixing layer depth. The updraft core number is
 398 critical for modeling plume top height and ground-level smoke concentrations.

399 The relative impacts of these coefficients on plume height (second to the last
 400 column of Table 1) were assigned following a Fourier Amplitude Sensitivity Test (FAST)
 401 applied to a larger set of model coefficients (Table 2) derived from an earlier version of
 402 Daysmoke. (Note that the coefficient names in Table 2 do not necessarily correspond to
 403 the coefficient names in Table 1.)

404

405 Table 2 Parameters used in the FAST sensitivity analysis for Daysmoke. The ranges
 406 shown for D_f , T_z , and V are relative changes.

Model	Parameter	Meaning	Average	Range	Unit
ETM	C_e	Entrainment coefficient	0.18	0.1-0.5	(-)
DPM	C_p	Plume detraining coefficient	0.03	0.01-0.2	(-)
	C_u	Air horizontal turbulence coefficient	0.15	0.1~0.2	(-)
	C_w	Air vertical turbulence coefficient	0.01	0.01~0.1	(-)
	K_x	Thermal horizontal mixing rate	1	1~1.5	km(m/s)/°C
	K_z	Thermal vertical mixing rate	1	1~1.5	km(m/s)/°C
	W_c	Plume-to-environment cutoff velocity	0.5	0.2~0.8	m/s
	w^*	Air induced particle downdraft velocity	0.01	0.01~0.02	m/s
	W_r	Large eddy reference vertical velocity	1	1~1.5	m/s
	W_0	Initial plume vertical velocity	Computed	5~15	m/s
	dT	Initial plume temperature anomaly	Computed	5~15	°C
	D_f	Effective diameter of flaming area	Computed	-25~25%	m
	N_c	Number of updraft core	1	1~20	(-)
	T_z	Atmospheric thermal lapse rate	Observed	-25~25%	°C/km
	V	Average wind speed	Observed	-25~25%	m/s

407

408 The FAST analysis was introduced by [30] as a method to vary input variables
409 simultaneously through their ranges of possible values following their given probability
410 density functions (i.e., values which have a greater probability are chosen more often).
411 All input parameters are assumed to be mutually independent and each is assigned a
412 different frequency, which determines the number of times that the entire range of values
413 is traversed. With each input parameter oscillating at a different characteristic frequency,
414 a different set of input parameter values is obtained for each model run with every value
415 used once. The mean and variance, which characterize the uncertainty due to the
416 variability of the input parameters, are calculated for model output parameters. Fourier
417 analysis of each output for all model runs is used to separate the response of the model to
418 the oscillation of particular input parameters. Summation of those Fourier coefficients
419 corresponding to a particular input parameter frequency and its harmonics determines the
420 contribution of that input parameter to the model output variances. Finally, by scaling the
421 relative contribution of the input parameters to the total variance, partial variances are
422 obtained, which show the sensitivity of model output parameters to the variation of
423 individual input parameters in terms of a percentage of the variance. The Fourier
424 coefficients corresponding to input parameter frequencies and their harmonics do not
425 account for the entire variance of the model outputs. The Fourier coefficients
426 corresponding to linear combinations of more than one input parameter frequency
427 account for the remaining fraction of the variance, which can be attributed to the
428 combined influences of two or more parameters.

429 Details of the FAST analysis for a prescribed burn can be found in [10]. FAST
430 results are shown in Figure 5. The ratio of partial variance of a parameter to total variance
431 varies from one hour to another throughout the simulation period, but it only slightly
432 affects the relative importance of this parameter to others. The results for two hours are
433 shown to indicate this variation. The 15 parameters can be divided into three categories in
434 terms of their importance. The first category includes the two most important parameters:
435 the plume entrainment coefficient and number of plume updraft cores. Their ratios are
436 about 35 and 26%, respectively, at 1400, and 35 and 32% at 1500. In other words, each
437 parameter contributes one fourth to one third to the total variance. The second category
438 includes three important parameters: the initial plume temperature anomaly, diameter of
439 flaming area, and thermal stability. Their ratios are about 10% at 1400 and vary between
440 6 and 12% at 1500. Thus, each contribute about one tenth to total variance on average.
441 The third category includes the remaining parameters, whose ratios are 1% or less. These
442 parameters are not important to Daysmoke plume rise simulation.

443 The outcome of the FAST analysis was a redesign of Daysmoke with unimportant
444 coefficients either pre-assigned or expressed in terms of other variables. The result is the
445 reduced number of coefficients shown in Table 1.

446

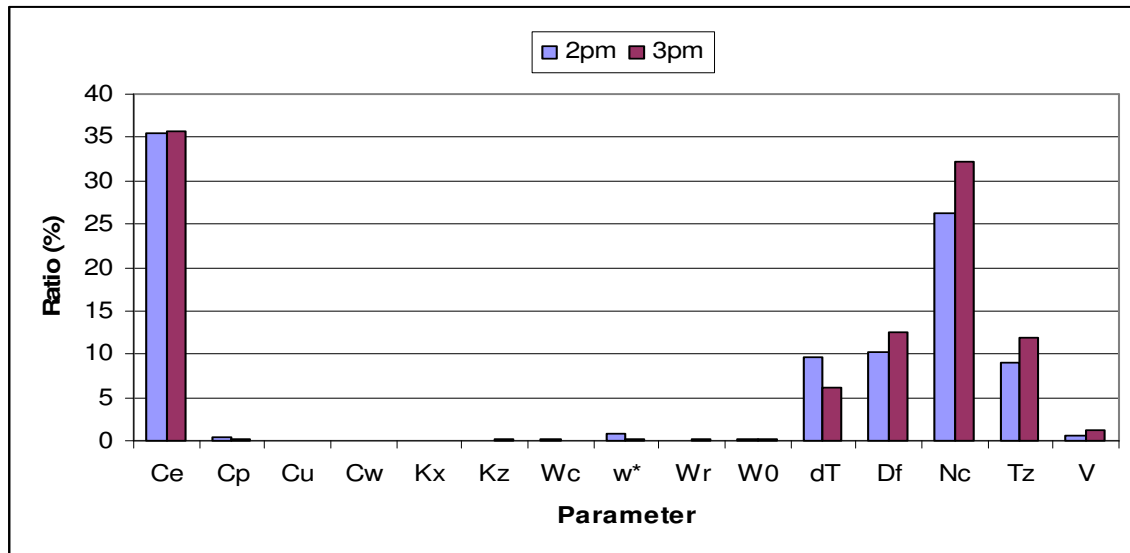
447

448

449

450

Figure 5. FAST sensitivity analysis of Daysmoke. The horizontal coordinate lists the model parameters (see Table 1 for their meanings). The vertical coordinate is the ratio (%) of partial variance of the parameter to total variance.



451

452

453

454

455

b) Input Data

456

457

458

Initial and hourly weather data include vertical profiles of temperature, three-dimensional components of the wind, and moisture (mixing ratio) for a location representative of the meteorology in the vicinity of the prescribed burn.

459

460

461

462

463

As regards initial values for the plume- D_0 , w_0 , and ΔT_0 , fire activity data include fuel type/amount (currently determined by National Fire Danger Rating System Fuel Model [31] the area burned, the location of the burn and the date/start time of the burn. In addition the Each firing technique: backing fire, strip-head fires, head fire, ring fire and aerial ignition [32] produces fires of differing intensity and spread rates.

464

465

466

467

468

469

470

471

472

473

The process of converting from this description of a prescribed burn to the required Daysmoke inputs proceeds in four basic steps: fuel consumption calculation, total emissions calculation, hourly emissions and determination of D_0 . The first three components are similar to those of the BlueSky Smoke Modeling Framework [33]. Total fuel consumption for each burn is determined using the single parameter regression equations for version 2.1 of CONSUME as given in appendix C of the User's Guide [34]. For each burn, total emissions for a number of chemical species are then calculated by multiplying the total consumed fuel by a species-specific emissions factor (Table 3). Values for the emissions factors are taken from the average emission factors of 26 intensively studied southeastern prescribed burns during 1995 and 1996 [35].

474

475

476

477

478

Hourly emissions are derived from this total value using the Emissions Production Model (EPM) [36] that derives time series of emissions and heat release for a fire based on a fairly simple source strength model. The time scale for completion of the flaming component is determined by the theoretical fire behavior. For a given wind speed, head/flanking/back fire spread rates are determined from BehavePlus [37] for the

479 appropriate NFDRS fuel model.
480

481 Table 3: Average emission factors from 26 southeastern prescribed fires.

<i>Chemical Species</i>	<i>Emission Factor (g/kg)</i>	
	Flaming Combustion	Smoldering Combustion
CO ₂	1,664.00	1,649.00
CO	82.00	106.00
CH ₄	2.32	3.42
C ₂ H ₄	1.30	1.30
C ₂ H ₂	0.50	0.48
C ₂ H ₆	0.32	0.46
C ₃ H ₆	0.51	0.59
C ₃ H ₈	0.09	0.11
C ₃ H ₄	0.05	0.05
NMHC	2.77	3.00
PM _{2.5}	11.51	10.45

482
483
484
485
486
487
488
489
490

The heat release rate (Q) is simply estimated as 50% of the product of the mass of fuel consumed per hour and the heat of combustion ($1.85 \times 10^7 \text{ J kg}^{-1}$) [38]. The assumed 50% reduction in the heat release rate is designed to restrict only a portion of the total heat released going into the plume with the other 50% going into the heating of surrounding vegetation and ground surface. The initial values for the plume - D_0 , w_0 , and ΔT_0 - can be related to the heat of the fire [39] by

$$491 \quad w_0 D_0^2 = \frac{4Q}{\pi C_p \rho \Delta T_0} \quad (15)$$

492
493
494
495
496
497
498

C_p is the specific heat ($\text{J kg}^{-1} \text{ K}^{-1}$), w_0 is the vertical velocity entering the plume (m s^{-1}), ρ is the air density (kg m^{-3}) and ΔT_0 is the temperature difference between the plume air and ambient conditions. Representative values for w_0 and ΔT_0 of 25 m s^{-1} and $40 \text{ }^\circ\text{C}$ can be assumed based on numerical simulations of coupled fire atmosphere models [39]. Using these assumed values for vertical velocity and temperature difference allows D_0 to be determined.

499 Equation (15) with the above specified initial conditions is assumed to be valid at
500 some reference height h_0 defined as the base of the plume where flaming gasses and
501 ambient air have been thoroughly mixed and where the incipient plume temperature ΔT_0
502 of $40 \text{ }^\circ\text{C}$ is found. For small prescribed burns, h_0 may be found approximately 10 m
503 above ground and for wildfires, h_0 may be found several 100's of meters above ground.
504 For a typical grassfire [40] h_0 can be found near 35 m.

505 The number of particles released per time step is determined from hourly
506 emissions derived from the total fuel consumption [34] using the Emissions Production
507 Model (EPM) of [36] modified for prescribed burns.

508

509 *c) Comparison with Briggs and LES model plumes*

510

511 [41] used a high-resolution large eddy simulation (LES) model to explore the
 512 dynamics of buoyant plumes arising from a heat source representative of wildland fires.
 513 The model was designed to resolve the majority of the turbulent eddies in the plume and
 514 its environment, and thus does not suffer from approximations inherent in simple
 515 empirical plume models. [42] compared mean plume trajectories from the LES model
 516 with the two-thirds law plume rise model of [29] and its modification by [43] to account
 517 for finite-area sources. They found that within the first kilometer downwind from the heat
 518 source the mean plume rise seen in the simulations was well-described by the power law
 519 trajectory and is in reasonably good agreement with simple plume rise calculations. The
 520 LES and Briggs results place narrow bounds on mean plume trajectories and therefore
 521 provide a critical validation test for Daysmoke.

522 A version of the Briggs formulation provided by [44], and modified by [45]
 523 allows for insertion of the initial values used for Daysmoke.

524

$$h = \left(\frac{3}{2e^2} \right)^{1/3} F^{1/3} x^{2/3} / U \quad (16)$$

525

where

$$F = \frac{g\Delta T_0 w_0^2 D_0^2}{4(T_e + \Delta T_0)}$$

526

527 Here,

528 x = the horizontal distance along the plume centerline downwind from the stack.

529 U = the mean horizontal wind speed (ms^{-1}) for the air layer containing the plume.

530 ΔT_0 = the plume temperature (K) anomaly.

531 w_0 = the stack gas ejection speed (ms^{-1}).

532 D_0 = the internal exit diameter (m) of the stack.

533 h = the height of the plume axis above the source (stack) (m).

534 e = the entrainment coefficient (conventionally, 0.66) for the Briggs model.

535 g = gravitational acceleration (ms^{-2})

536 T_e = plume exit temperature (K)

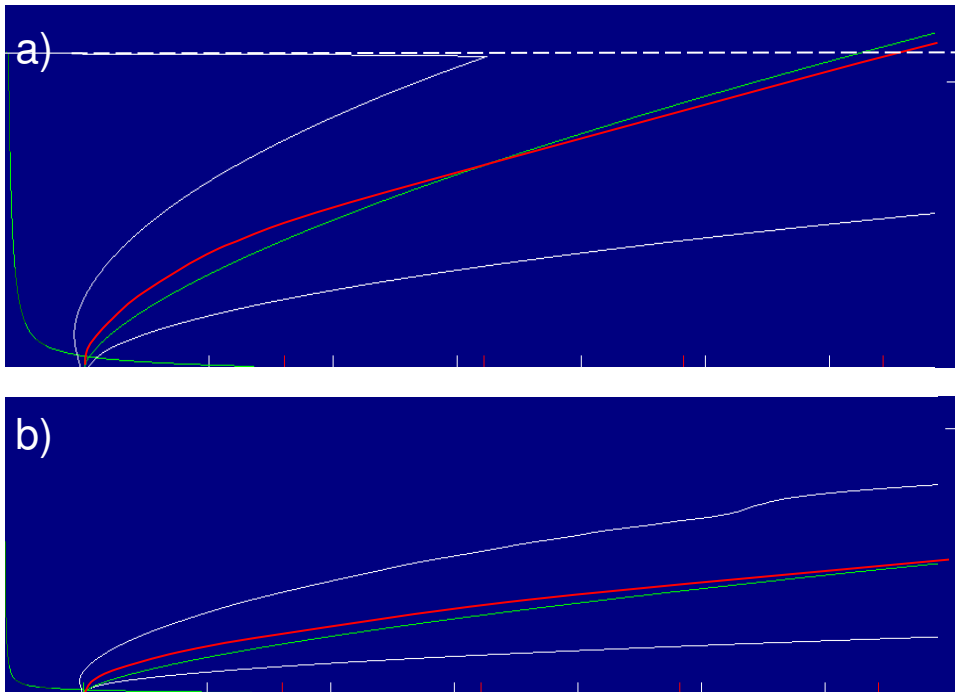
537

538 Daysmoke was run with a test profile of temperature and wind created from a
 539 WRF generated sounding for Ft. Benning, GA, for 23 January 2009. All winds below
 540 1700 m were set to blow from the west with a speed of $U=9.0 \text{ ms}^{-1}$ as the Briggs theory is
 541 set for a layer mean wind speed. The outcome of the comparison for the first seven
 542 kilometers downwind is shown in Figure 6. Plume boundaries calculated via Equation (5)
 543 are shown by the white lines. The green lines identify mean plume trajectories from the
 544 Briggs two-thirds law for a neutral atmosphere. For the initial effective plume diameter
 545 $D_0=62\text{m}$ (Figure 6a), the Daysmoke plume, driven by the hyperbolic vertical velocity
 546 profile (alternating dark and light green lines at the left side of the figure), rose more
 547 steeply during the first 500 m downwind. Then the centerline for the Daysmoke plume
 548 declined from 60 m above the Briggs trajectory at 500 m downwind to intersecting the
 549 Briggs trajectory at 3.2 km downwind. The outcome was a more highly bent-over plume.
 Beyond 3.2 km, the Daysmoke centerline ran slightly below the Briggs trajectory – 15 m

550 below where the centerlines crossed the mixing height (dashed line) at 7.3 km downwind
 551 from the ignition site.

552

553 Figure 6. Daysmoke-simulated plume boundaries (white lines), Daysmoke plume
 554 centerline (red lines), and Briggs-calculated mean plume trajectories (green lines) for a)
 555 $D_0=62\text{m}$ and b) $D_0=17\text{m}$. The mixing height is given by the dashed line.



556

557 Similar results were found for the smaller $D_0=17.0\text{m}$ plume (Figure 6b). This
 558 Daysmoke plume initially rose more steeply than the Briggs trajectory for the first 150 m
 559 downwind placing the plume approximately 25 m above the Briggs trajectory. Then the
 560 two curves gradually converged past 7.5 km downwind.

561

562 It is apparent that the Daysmoke plumes are initially more vigorous but, overall,
 563 the plume rise is well-explained by the power-law trajectory. The differences are minimal
 564 in comparison with the area swept out by the plume boundaries.

564

565 **4. Model Evaluation (Study of Weak Plumes)**

566

567 During 2008-2009, a smoke project was conducted at Fort Benning, GA. The site
 568 was chosen because of the large size of its prescribed burn operation and the
 569 aggressiveness of its burn program – typically a 1-3 yr fire return interval. Burning when
 570 fuel loadings had increased to just carry fire would not be expected to release heat
 571 sufficient to loft a towering plume. Daysmoke simulations produced some plumes that
 572 ascended to the mixing height. Other simulated plumes rose partway through the mixing
 573 layer before losing identity as a plume – breaking up and being redistributed by
 574 convective circulations.

575

576 The project collected data on plume top height and ground-level $\text{PM}_{2.5}$ - both
 577 critical data sets for validation of Daysmoke – for eleven burns. Three mobile trucks,
 each equipped with pairs of DustTrak real-time $\text{PM}_{2.5}$ samplers (Liu 2010), were operated

578 at distances of roughly 1 mile, 2 miles, and 4 miles downwind from the burn. The trucks
 579 were moved when wind shifts created the necessity to relocate beneath the smoke
 580 plumes. An example of the truck protocol is shown in Figure 7. The three trucks (color
 581 coded) were moved to various positions during the burn to maintain location under the
 582 plume (shown schematically by the parabolic boundaries) as judged by the truck crews.
 583 PM_{2.5} observations by the DustTrak samplers were corrected for wood smoke by
 584 multiplying by a factor of 0.275.

585 Daysmoke was run with hourly vertical profiles of wind, humidity, and
 586 temperature from high-resolution weather simulations by the WRF model. Emissions
 587 data were provided by the methodology described in *c) Input Data* above.

588 Our analysis placed the eleven burns in five categories (Table 4). The first column
 589 shows that three burns fell into the first category - ground-level smoke concentrations
 590 increased with distance from the burn. Plume statistics are summarized in Figure 8.
 591 Daysmoke contains stochastic terms for convective circulations that are set so they
 592 cannot be repeated. Thus successive Daysmoke runs will give slightly different answers.
 593 To smooth out the effects of the stochastic terms, we constructed ensemble averages of
 594 five simulations. The averages of the residuals (defined as the differences between
 595 ensemble averages and observed PM_{2.5}) for the periods of the burns (defined as time of
 596 ignition until completion of ignition) for the three days are shown by the squares in
 597 Figure 8. The spreads of residuals are given by the horizontal bars connected by the
 598 vertical lines. Average residuals for all three trucks ranged less than +/- 5 μgm^{-3} . The
 599 magnitudes of the spreads for Truck1 and Truck 2 never exceeded 10 μgm^{-3} . Given
 600 uncertainties in defining updraft core number and model errors in wind speed and
 601 direction, the results for the first category of Table 4 are as good as can be expected from
 602 an empirical-statistical model like Daysmoke.

603

604 Table 4. Fort Benning burns listed by plume characteristics

Increase	Decrease	Extreme Decrease	Out Of Plume	Misc
3	3	2	2	1
09 Apr 08	14 Apr 08	15 Jan 09	13 Jan 09	14 Jan 09
21 Jan 09	15 Apr 08	23 Jan 09	20 Jan 09	
08 Apr 09	09 Apr 09			

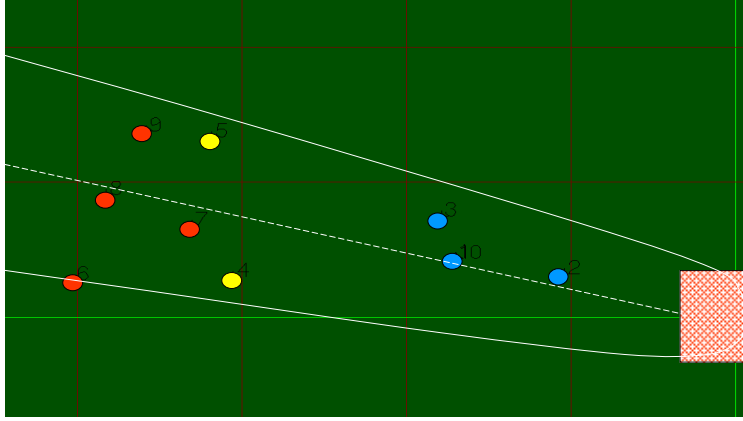
611 The results for the second category of Table 4 – ground-level smoke
 612 concentrations decreased with distance from the burn - are shown in Figure 9. Daysmoke
 613 slightly under-predicted smoke at Truck 1 and over-predicted smoke at Truck 2 and
 614 Truck 3. The discrepancies are small – less than 10 μgm^{-3} . Spreads also were small at all
 615 three trucks; the largest being 21 μgm^{-3} .

616 The third column of Table 4 lists the two days with plumes characterized by very
 617 high concentrations of smoke at Truck 1 and very steep gradients of smoke concentration
 618 between the trucks (Figure 10). Daysmoke greatly under-predicted burn event smoke at
 619 Truck 1 – minus 60 μgm^{-3} with a spread ranging from -32 to -89 μgm^{-3} . The average
 620 residual was improved for Truck 2 (-12 μgm^{-3}) but the spread remained high (-47 to 22
 621 μgm^{-3}). The better results at Truck 3 could be explained by the truck being located near

622 the edges of the plumes.

623

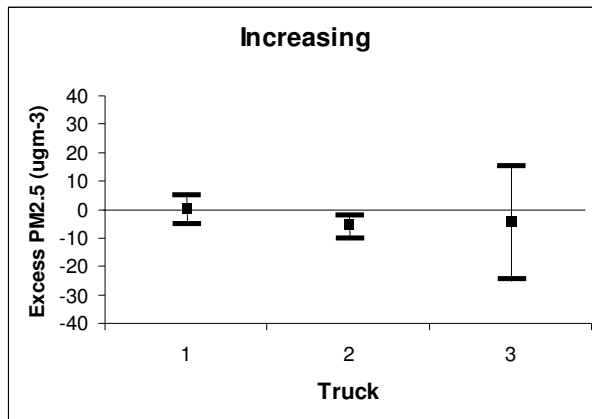
624 Figure 7. Positions of three trucks: Truck 1 (blue), Truck 2 (yellow), and Truck 3 (red)
625 during the 9 April 2008 prescribed burn at Fort Benning. Grid outlines one mile squares.



626

627

628 Figure 8. Ensemble average Daysmoke minus observed $PM_{2.5}$ (squares) at the three
629 trucks for the three days when smoke concentrations increased with distance. The spreads
630 of the departures are shown by the horizontal bars.



631

632

633 The fourth and fifth columns of Table 4 list those days characterized by,
634 respectively, truck locations away from the plume (either no roads or movement
635 restricted by military activities) and corrupted or lost data.

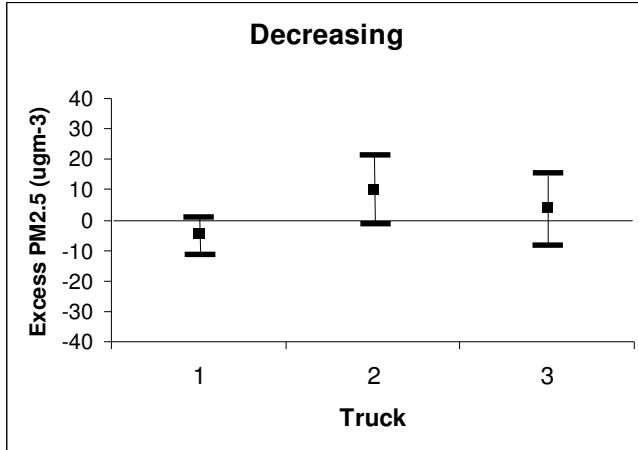
636

637 The poor results from Daysmoke for the events characterized by high smoke
638 concentrations at Truck 1 and steep gradients of $PM_{2.5}$ between the trucks (column 3 of
639 Table 4) needs further explanation. That these two events were extraordinary is shown by
640 peak 30-s $PM_{2.5}$ for the seven days for which complete data are available for all three
641 trucks (Figure 11). Peak $PM_{2.5}$ exceeding $600 \mu\text{g m}^{-3}$ for 15 January and 23 January 2009
642 imply that Truck 1 was located within the ascending plume on both days while Truck 2
643 and Truck 3 were located within particulate matter detrained from the plume as it passed
644 overhead. This implication contrasts with Daysmoke solutions for the other days that
placed the trucks either within detrained smoke or within remnants of the smoke plume

645 torn apart and down-mixed by convective circulations.

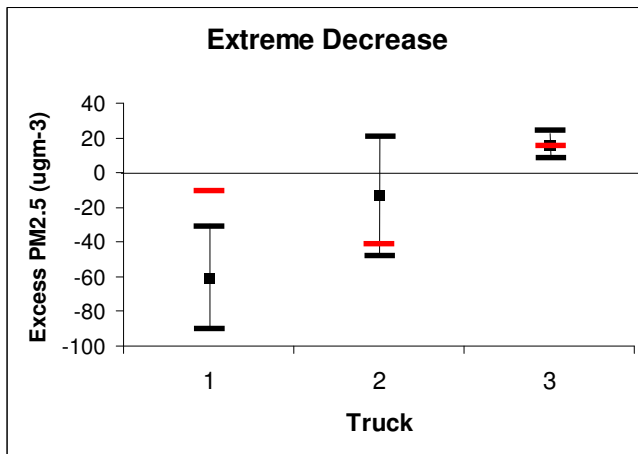
646

647 Figure 9. Ensemble average Daysmoke minus observed $\text{PM}_{2.5}$ (squares) at the three
 648 trucks for the three days when smoke concentrations decreased with distance. The
 649 spreads of the departures are shown by the horizontal bars.



650

651 Figure 10. Ensemble average Daysmoke minus observed $\text{PM}_{2.5}$ (black squares) at the
 652 three trucks for the two days of high smoke concentrations at Truck 1 and steep gradients
 653 of smoke between the trucks. The spreads of the departures are shown by the horizontal
 654 bars. Red bars: Daysmoke minus observed $\text{PM}_{2.5}$ for a highly tilted plume for 23 January
 655 2009.



656

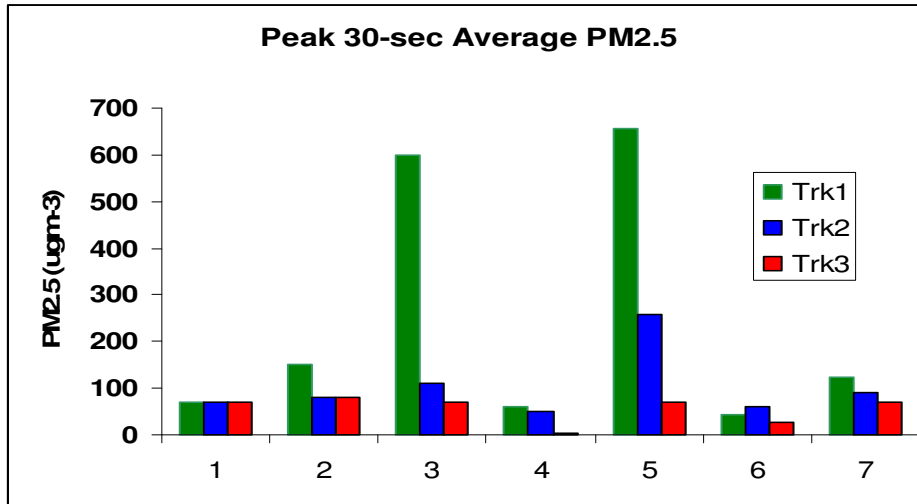
657 Given the initial conditions of $w_0 = 25 \text{ m sec}^{-1}$ and $\Delta T_0 = 40 \text{ C}$, no choice for
 658 updraft core number could produce both the very high smoke concentrations at Truck 1
 659 nor the steep gradients of $\text{PM}_{2.5}$ between the other trucks. Therefore the Daysmoke bent-
 660 over plume solution failed to reproduce the events of 15 January and 23 January 2009.

661 We varied the initial conditions subject to the constraint that the flux, given by the
 662 product of the initial velocity with the square of the initial effective plume diameter, was
 663 held constant. The top panel of Figure 12 shows the bent-over solution for a 1-core
 664 updraft plume for 23 January 2009. We reduced the initial conditions to $w_0 = 0.5 \text{ m sec}^{-1}$
 665 and $\Delta T_0 = 1.0 \text{ C}$ to obtain the solution for a “highly tilted” plume (middle panel of
 666 Figure 12). Conservation of total flux required increasing the initial effective plume

667 diameter from 59 m to 417 m – a requirement that decreases the impact of entrainment on
 668 the plume. Thus the weakly buoyant highly-tilted plume was driven almost entirely by
 669 buoyancy and was capable of growth through the depth of the mixing layer.

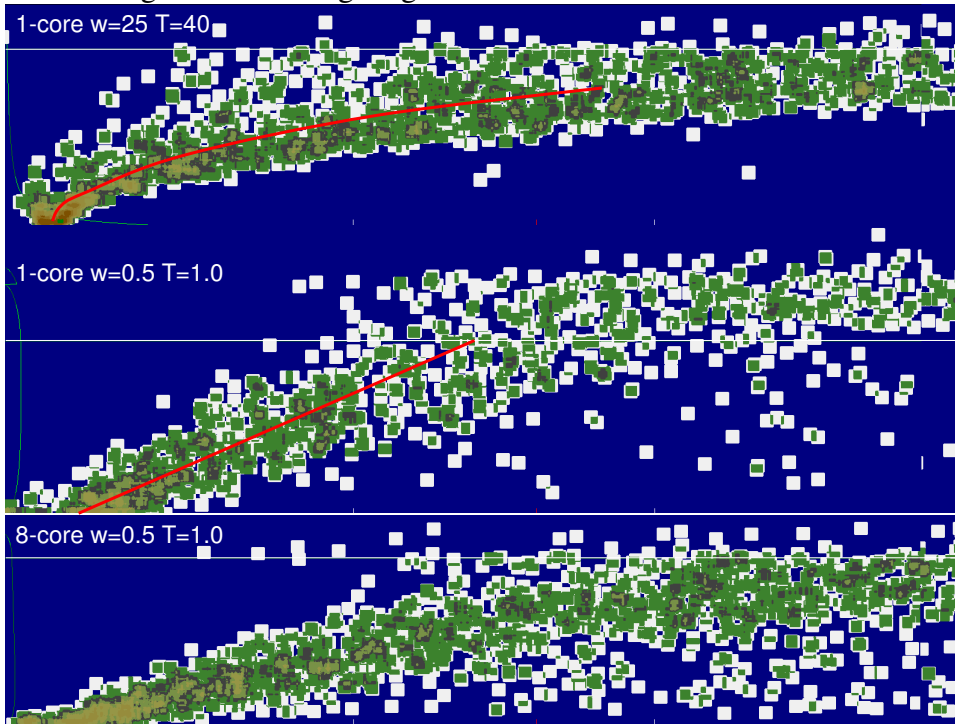
670

671 Figure 11. Peak 30-sec averaged $PM_{2.5}$ for seven complete data sets from the 2008-2009
 672 smoke project at Fort Benning, GA. The burn dates are: (1) 9 APR 2008, (2) 14 APR
 673 2008, (3) 15 JAN 2009, (4) 21 JAN 2009, (5) 23 JAN 2009, (6) 8 APR 2009, and (7) 9
 674 APR 2009.



675

676 Figure 12. Daysmoke plumes for three selections of initial conditions. The horizontal
 677 white line gives the mixing height.



678

679

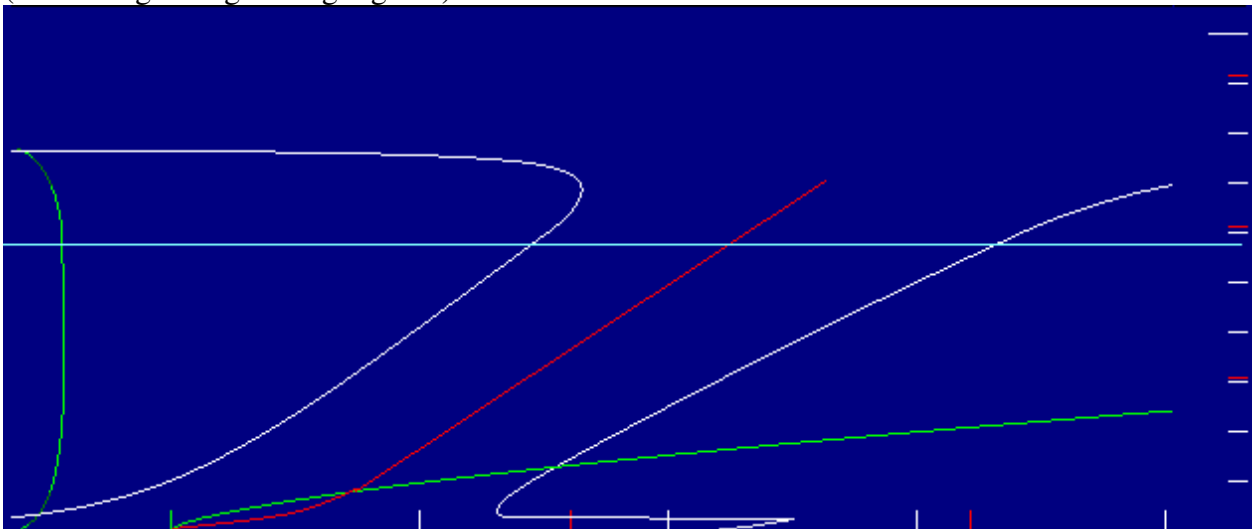
680 The plume axis is characteristically quasi-linear as compared with the parabolic
 681 axis of the bent-over plume (upper panel). Running Daysmoke with the updraft core

682 number set to eight (estimated for this burn) yielded the highly tilted plume solution
 683 shown in the lower panel of Figure 12. Note how this plume runs along the ground before
 684 ascending. The plume tilt of 15 degrees is greater than that for the 1-core plume (middle
 685 panel) and the plume is confined to the mixing layer. The red bars in Figure 10 show that
 686 the 30-min averaged $\text{PM}_{2.5}$ difference between Daysmoke and observed smoke
 687 concentration at Truck 1 of $-8 \mu\text{gm}^{-3}$ was greatly improved over the $-89 \mu\text{gm}^{-3}$ calculated
 688 for the bent-over plume. Results for Truck 2 and Truck 3 showed minor changes from the
 689 original differences for 23 January 2009.

690 Is the highly-tilted plume represented by Briggs theory? Figure 13 shows plume
 691 boundaries (white lines) for the 23 January 2009 simulation (aspect ratio: $\Delta x/\Delta z = 2$). The
 692 plume axis (red line) describes a plume that runs along the ground for approximately 0.6
 693 km then rises at approximate 3.5 ms^{-1} (dark green/light green line) along a quasi-linear
 694 axis. The weak buoyancy of the plume, shielded from entrainment by its 417 m diameter,
 695 ascended to the mixing height 2 km downwind and rose 100 m above the mixing layer
 696 (light blue line). The Briggs solution (Equation 16), shown by the green line, has the
 697 plume ascending to 250 m 4 km downwind from the burn.

698

699 Figure 13. Plume boundaries (white lines) for the highly-tilted plume simulated by
 700 Daysmoke for the 23 January 2009 prescribed burn. Other lines are: plume axis (red), the
 701 Briggs solution (green), the mixing height (light blue), and the plume vertical velocity
 702 (alternating dark green/light green).



703

704

705 Is there independent evidence to support the Daysmoke solution for the highly-
 706 tilted plume? Figure 13 shows stack and cooling tower plumes from an electric power
 707 generating station. The stack plume shows the strongly bent-over parabolic structure (red
 708 line) typical of relative high velocity effluents rapidly slowed by entrainment on ejection
 709 through a relatively small plume diameter. The cooling tower plume, tilted along a linear
 710 axis (blue line), is characteristic of low velocity effluents ejected within a relative large
 711 plume diameter and driven by buoyancy. The plume structures modeled with Daysmoke
 712 compare favorably with the plumes shown in Figure 14.

713

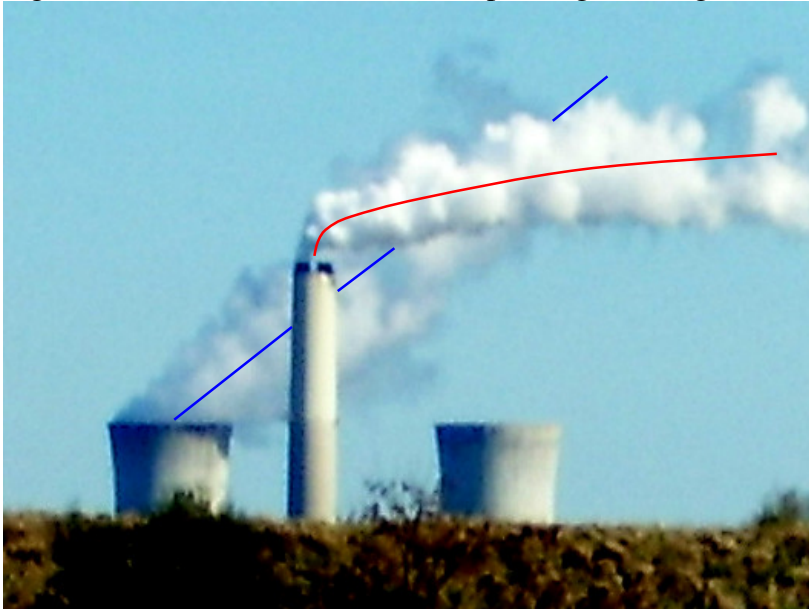
714

Plume top heights (squares) and height ranges (connecting lines) for plumes
 simulated by Daysmoke (red squares in Figure 15) compare favorably with plume top

715 heights measured by ceilometer (black squares). Relative to the observed lower range,
 716 Daysmoke plume tops were on the average 8 m high. However, relative to the observed
 717 higher range, Daysmoke plume tops were on the average -200 m low. Thus Daysmoke plume
 718 tops were, overall, slightly low.

719

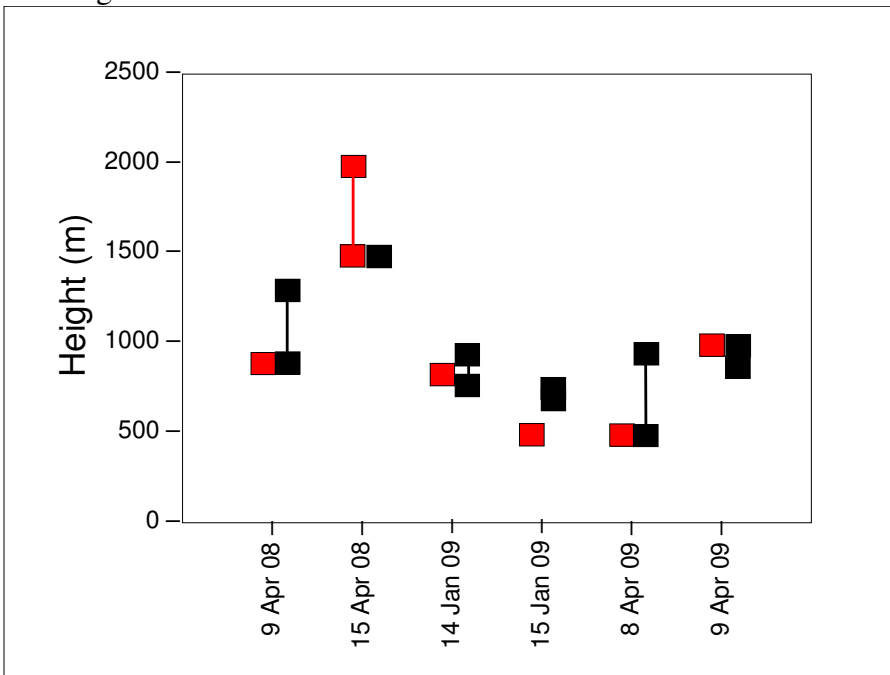
720 Figure 14. Plumes from an electrical power generating station.



721

722

723 Figure 15. Plume heights for Daysmoke-simulated plumes (red squares) compared with
 724 plume heights observed by ceilometer (black squares) for six prescribed burns at Fort
 725 Benning.



726

727

728

729 **5. Model Application (CMAQ)**

730
731 An adaptive grid version of CMAQ (AG-CMAQ) has been recently developed to
732 better resolve the processes involving plumes [20] AG-CMAQ integrates the adaptive
733 grid algorithm of [47] into CMAQ 4.5 and is based on the adaptive grid air pollution
734 model described in [11] [12]. AG-CMAQ employs r-refinement: the number of grid cells
735 remains constant but grid nodes are moved to cluster in areas where plumes are detected.
736 Although the nodes are relocated, their connectivity does not change and the structure of
737 the grid is maintained. In AG-CMAQ, a curvilinear coordinate system is fitted to the
738 adapted non-uniform grid and, using coordinate transformations, the governing equations
739 are transformed to a space where the grid is uniform. Then the transformed equations are
740 solved in this space by directly applying the CMAQ solution algorithms that are designed
741 for uniform grids. A variable time-step algorithm [48] allows each cell in AG-CMAQ to
742 be assigned a unique local time-step and was included in the model to improve
743 computational efficiency.

744 The objective of grid adaptation in AG-CMAQ is to achieve more accurate
745 representations of spatial fields by increasing grid resolution at locations where the error
746 in numerical solutions is largest. The adaptation is achieved by estimating a weight
747 function that efficiently quantifies numerical error and clustering grid nodes within the
748 regions that result in the highest weights. The initial application of AG-CMAQ
749 attempted to model biomass burning plumes impacting air quality in the Atlanta
750 metropolitan area [20]. For that simulation, the Laplacian of the concentration of primary
751 particulate matter from biomass burning was used as a weight function. Comparison of
752 AG-CMAQ's performance to that of the static grid CMAQ model indicated that grid
753 adaptation resulted in reduced numerical diffusion, better defined plumes, and closer
754 agreement with site measurements. Here, we describe an application of AG-CMAQ to
755 model prescribed burn plumes at Fort Benning, GA using information provided by
756 Daysmoke.

757 Daysmoke can be applied as an emissions injector for AG-CMAQ in the same manner
758 as it has been previously used with CMAQ. Detailed information describing plume rise or
759 vertical distribution of buoyant prescribed burn emissions is necessary to achieve realistic
760 results with gridded photochemical models that typically lack the mechanisms necessary
761 to simulate this process. The fire emissions are injected into CMAQ's vertical layers
762 following the vertical pollutant profile produced by Daysmoke at a downwind distance
763 that allows full plume development. The location at which the emissions are injected
764 within the horizontal CMAQ domain is not a straightforward choice. Injecting the
765 emissions at the fire emissions source implies that a vertical profile modeled downwind
766 of the fire is applied further upwind at the location of initial release. On the other hand,
767 injection of emissions downwind at the location where the plume's fully developed
768 vertical profile was estimated with Daysmoke entails neglecting chemistry and aerosol
769 processes included in CMAQ but absent from Daysmoke up to this downwind distance.
770 The error from either choice is greater as the downwind distance necessary to achieve a
771 fully developed vertical plume profile increases relative to grid resolution. Plumes that
772 rapidly reach their maximum plume rise and vertically distribute pollutants may not bring
773 forth significant errors. However, given that full plume development may occur at
774 distances larger than 15 km and grid resolution in CMAQ has been previously taken

775 down to 1 km, this might not necessarily be the case. The significance of this issue is
 776 even greater in AG-CMAQ, where an initial increase in resolution around the source of
 777 emissions is meant to enhance chemical and physical processes shortly after release. In
 778 the future, a tighter coupling of Daysmoke with AG-CMAQ should address these issues.

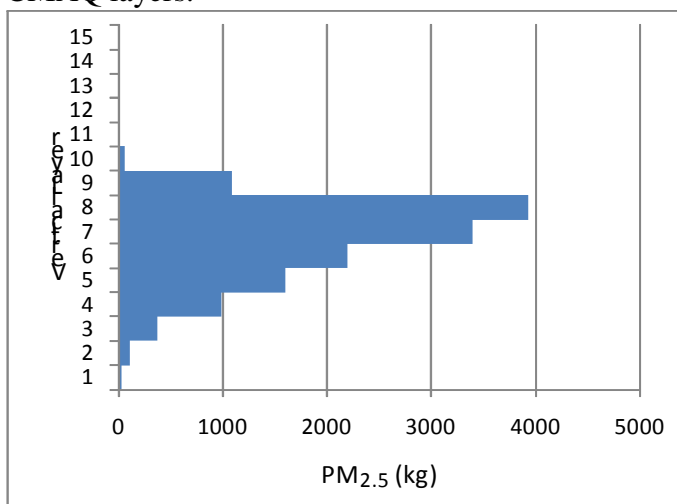
779 In the following application we have modeled the effects on air quality from a
 780 prescribed burn at Fort Benning, GA on April 9, 2008. During this day, 300 acres of
 781 wildland were treated. Ignition occurred at 16:30 GMT and flaming continued until 18:45
 782 GMT, with smoldering emissions continuing thereafter. This episode is of particular
 783 interest because peaking $PM_{2.5}$ concentrations were recorded at the Columbus, GA airport
 784 air quality monitoring site, possibly due to the impact of the burn, providing an
 785 opportunity to compare modeled results to those observed at a regulatory network station.

786 Hourly emissions from the prescribed burn were estimated with the Fire Emission
 787 Production Simulator (FEPS) [49] using information provided by land managers at the
 788 site. Background emissions for the photochemical simulations were prepared using the
 789 Sparse Matrix Operator Kernel Emissions model (SMOKE, version 2.4) [50] with a 2002
 790 “typical year” emissions inventory [51] projected to year 2008 using the existing control
 791 factors and the growth factors generated from the Economic Growth Analysis System
 792 (EGAS) Version 4.0. Meteorological data is provided through the Weather Research and
 793 Forecasting model (WRF, version 3.1) [52] at 1.333 km resolution and 34 vertical layers
 794 of increasing depth from the surface to the top. Initialization, boundary conditions
 795 constraining, and nudging at 6 hour intervals were performed using analysis products
 796 from the North American Mesoscale (NAM) model. The CMAQ domain covered 120 x
 797 124 km over southwestern Georgia and southeastern Alabama with a 1.333 km horizontal
 798 grid spacing and 34 vertical layers.

799 Daysmoke simulations were undertaken using 6-updraft cores. For fire emissions
 800 injection into CMAQ we used the vertical plume profile estimated by Daysmoke 4 km
 801 downwind of the fire, and applied it at the location of the fire in the CMAQ domain. This
 802 length provided sufficient time for full plume development and was not exceedingly
 803 distant from the source (3 grid cells downwind). The vertical distribution of $PM_{2.5}$ fire
 804 emissions for the entire episode is shown in Figure 16.

805

806 Figure 16. Vertical distribution of prescribed burn $PM_{2.5}$ emissions into CMAQ and AG-
 807 CMAQ layers.



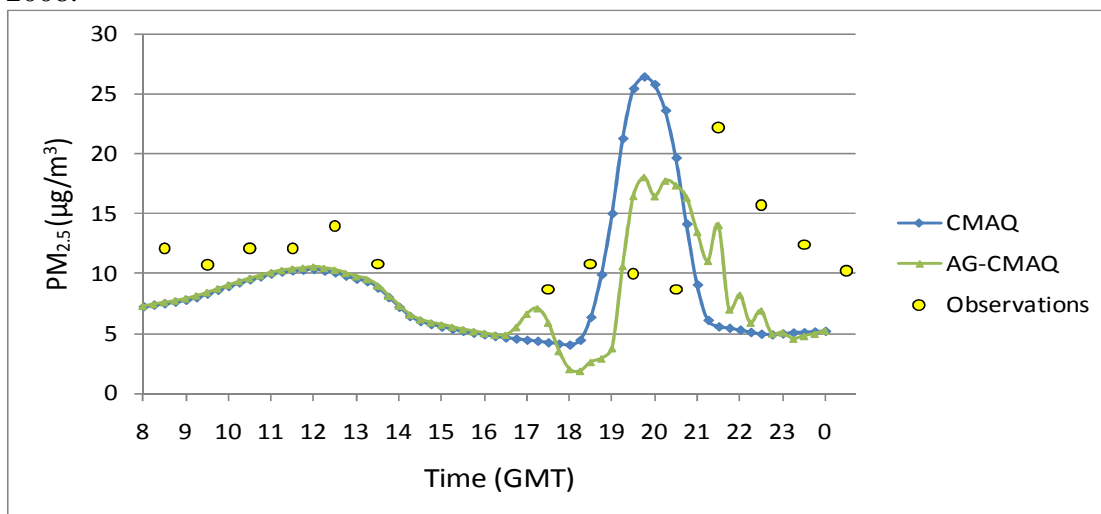
808

809 The largest fraction of emissions is injected into layer 8, which spans an altitude
 810 from approximately 500m to 680m above the ground. Nearly 70 % of fire emissions were
 811 distributed into layers 6, 7, and 8 which extend from approximately 335m to 680m above
 812 the ground. The same procedure was applied for fire emissions injection in the AG-
 813 CMAQ simulation. Grid adaptation was driven by the curvature in the fire emitted $PM_{2.5}$
 814 concentration field.

815 Figure 17 shows the time evolution of $PM_{2.5}$ concentration at the Columbus
 816 Airport monitoring site 30 km from the location of the prescribed burn for both the
 817 CMAQ and AG-CMAQ runs, as well as available observational data. CMAQ
 818 overestimates the peak concentration while AG-CMAQ underestimates this value.
 819 However, the magnitude of the error in the maximum $PM_{2.5}$ level for both models is
 820 approximately the same ($4 \mu\text{g}/\text{m}^3$). A sharp increase in concentration is perceived in the
 821 observations after 21:00 UTC. Similarly, rapid increments are perceived in the CMAQ
 822 and AG-CMAQ simulations, although occurring at earlier times. The CMAQ modeled
 823 $PM_{2.5}$ concentrations fall abruptly after peaking, while the decrease is gentler with AG-
 824 CMAQ and more closely resembles that seen in the observations. Throughout the
 825 simulation, the mean fractional error in the modeled results relative to station
 826 observations was reduced by 17 % on average using AG-CMAQ compared to CMAQ. A
 827 timing mismatch in observed and modeled peak pollutant levels is also evident. The fact
 828 that emissions estimated by FEPS are hourly starting at the top of the hour and ignition
 829 actually occurred 30 minutes past 16:00 GMT may at least partially account for the
 830 discrepancy.

831

832 Figure 17. Hourly averaged $PM_{2.5}$ concentrations ($\mu\text{g}/\text{m}^3$) as observed and modeled by
 833 CMAQ and AG-CMAQ at the Columbus airport air quality monitoring site on April 9,
 834 2008.

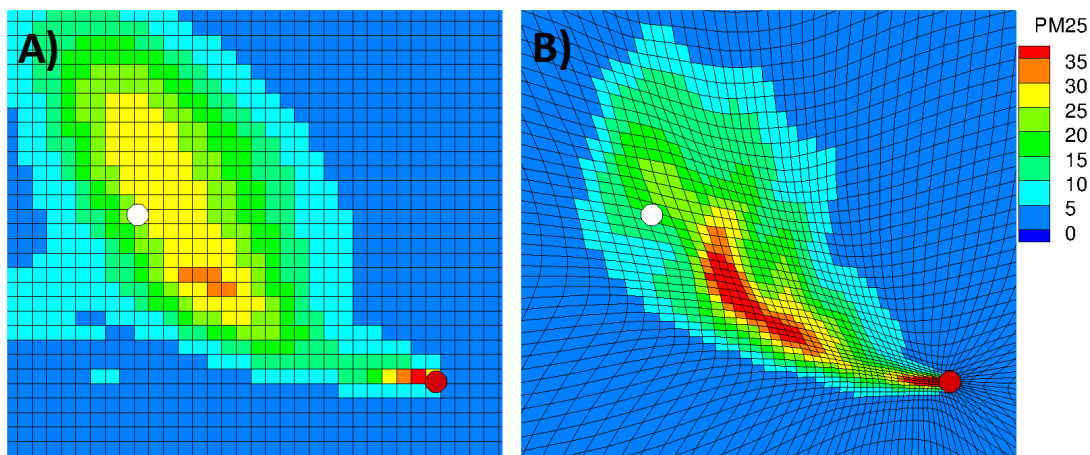


835

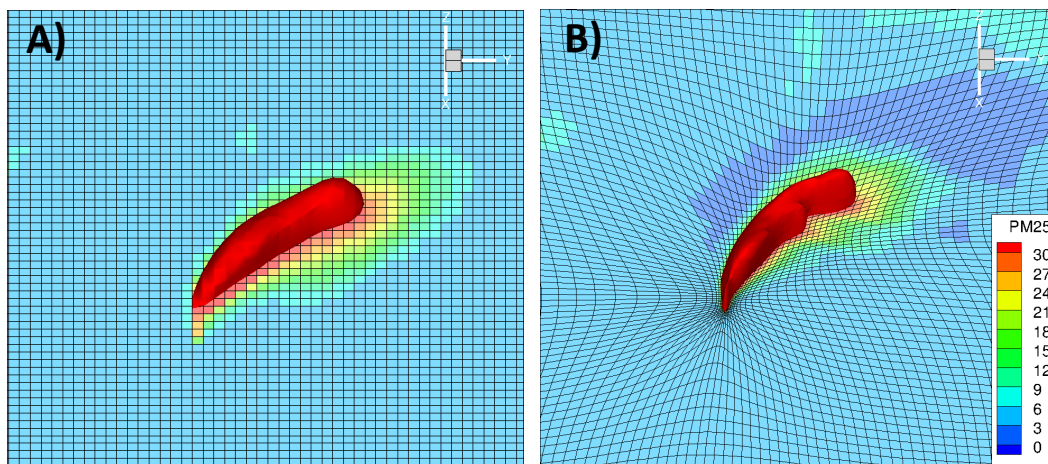
836 Better understanding of the modeled results can be gained from the pollutant
 837 concentration fields shown in Figure 18. These pollutant fields correspond to the instance of
 838 maximum concentration at the Columbus airport location. The static grid CMAQ
 839 plume appears more diffused, relative to that produced with AG-CMAQ. It is also
 840 apparent that impact at the airport site is not direct, but rather a tangential hit. The
 841 pollutant field from the AG-CMAQ simulation shows a more concentrated plume with
 842 higher pollutant levels near a core that has persisted longer into the simulation.

843 Significant grid refinement occurs at the source of emissions as well as along the plume
 844 centerline. The area surrounding the airport site also experiences appreciable refinement
 845 throughout the run. Figure 19 further contrasts the plumes produced with CMAQ and
 846 AG-CMAQ. These three-dimensional $\text{PM}_{2.5}$ concentration plots show surface level
 847 concentrations as well as a 3D plume volume defined as a constant concentration surface
 848 for concentrations larger than $30 \mu\text{g}/\text{m}^3$. The viewer position has been rotated to a 45°
 849 angle to better appreciate the plume volumes. From the images is it noticeable that the
 850 plume produced in the AG-CMAQ simulation offers a greater level of detail and is likely
 851 able to pick up finer details of the wind field to which it is subjected. The plume
 852 structures, undoubtedly, are highly dependent on the vertical pollutant distribution
 853 information provided by Daysmoke.

854
 855 Figure 18. Simulated $\text{PM}_{2.5}$ concentrations ($\mu\text{g}/\text{m}^3$) on April 9, 2008 at 19:45 GMT using
 856 A) CMAQ and B) AG-CMAQ. Locations of the prescribed fire at Ft. Benning and the
 857 Columbus airport air quality monitoring site are indicated by red and white circles
 858 respectively.



859
 860 Figure 19. Three-dimensional views of $\text{PM}_{2.5}$ concentrations ($\mu\text{g}/\text{m}^3$) on April 9, 2008 at
 861 19:15 GMT using A) CMAQ and B) AG-CMAQ.



862
 863
 864

865

866 **6. Summary**

867

868 In this paper we have presented the plume rise and dispersion model Daysmoke,
869 intended for the simulation of smoke plumes from wildland fires. The model theory
870 presented in this paper is the outcome of a former version that was subjected to a
871 sensitivity analysis with the Fourier Amplitude Sensitivity Test (FAST). The FAST test
872 identified empirical parameters important for plume height prediction. Therefore, many
873 empirical coefficients have been pre-assigned or expressed in terms of other variables.

874 We compared Daysmoke plumes with Briggs theory and found good agreement
875 for “bent-over” plumes although the two-thirds theory is not explicit in Daysmoke.
876 However, the solutions for “highly-tilted” plumes characterized by weak buoyancy, low
877 initial vertical velocity, and large initial plume diameter do not match Briggs theory.

878 We further evaluated Daysmoke by comparing simulations and observations of
879 $PM_{2.5}$ and plume height for weak plumes from eleven prescribed burns at Fort Benning,
880 GA. Simulations of ground-level $PM_{2.5}$ compared favorably with observations taken from
881 three mobile trucks out to a distance of eight kilometers. Daysmoke plume tops were
882 found near the lower end of the range of observed plume tops for six prescribed burns.

883 Daysmoke simulated vertical smoke profiles for initializing smoke concentration
884 predictions from CMAQ (with and without and adaptive grid). These results show the
885 detail and accuracy that can be obtained at the regional scale.

886 Finally, it has been assumed that smoke plumes from wildland fires are just
887 complex combinations of “bent-over” plumes. Further research may establish that many
888 plumes from wildland fires are better characterized by “highly-tilted” plumes. In
889 addition, analyses just beginning of smoke observations of “strong plumes” from 56
890 prescribed burns should reveal the extent to which smoke from southern prescribed burns
891 done by mass ignition penetrates above the mixing layer. In these events, a fraction of
892 smoke emissions may not be available for dispersion locally downwind thus lowering
893 threats to air quality below those predicted. However, smoke trapped within the free
894 atmosphere above the mixing layer may be transported at different wind directions and
895 speeds to be reintroduced into the mixing layer at unexpected locations.

896

897 **Appendix A**

898

899 A string of two-dimensional mass conservative sinusoidal circulation cells
900 oriented normal to the mean wind vector within the mixing layer and with a translation
901 speed equal to the mean wind vector describe the convective boundary layer. The cells
902 are mutually independent – velocity amplitude, phase, wavelength and time history may
903 differ. The equations for convective circulations at each particle location (x, y, z) are:

$$w_{le} = w_e A \cos\left[\frac{\pi}{Ch}(r - St)\right] \sin\left(\frac{\pi z}{h}\right)$$

$$U_{le} = w_e C A \sin\left[\frac{\pi}{Ch}(r - St)\right] \cos\left(\frac{\pi z}{h}\right)$$

where

$$A = \sin\left[\frac{\pi}{c_1}(t + c_2) + c_3 C_n\right]$$

$$904 \quad r = (x^2 + y^2)^{1/2} \quad (A1)$$

and

$$u_{ce} = U_{le} u_m / S$$

$$v_{ce} = U_{le} v_m / S$$

$$w_{ce} = w_r \frac{h}{1000}$$

905

906 The variable, w_r (ms^{-1}), is the reference rotor velocity for convective eddies if the mixing
 907 layer depth is 1 km; h (m) is the depth of the mixing layer; u_m , v_m , and S are, respectively,
 908 the mean u-component and mean v-component for the mixing layer, and the transport
 909 wind speed. C is a shape factor, here set to 1.0 so that the convective eddies will have
 910 equal horizontal and vertical dimensions. The constants, c_1 , c_2 , and c_3 are amplitude
 911 weights: $c_1 = 1200$ sets the lifetime of a convective eddy to 20 minutes, $c_2 = 2117$ and c_3
 912 $= 23$ multiplies C_n (a set of 10 randomly selected numbers that range from 0-9). Many
 913 choices for c_2 and c_3 are possible. The selections are made so that adjacent eddy cells will
 914 have different time and amplitude histories.

915

916 Acknowledgements

917

918 The study is funded in part of the Southern Regional Models for Predicting Smoke
 919 Movement Project (01.SRS.A.5) funded by the USDA Forest Service National Fire Plan,
 920 the Joint Fire Sciences Program of the USDA and Department of Interior (JFSP 081606
 921 and JFSP 081604), the Department of Energy-Savannah River Operations Office through
 922 the USDA Forest Service Savannah River under Interagency Agreement DE-AI09-
 923 00SR22188, the National Research Initiative Air Quality Program of the Cooperative
 924 State Research, Education, and Extension Service, U.S. Department of Agriculture,
 925 (Agreement No. 2004-05240), and the U.S. Department of Defense through the Strategic
 926 Environmental Research and Development Program (SERDP-RC-1647).

927

928 References

929

930 1. SRFRR. *Southern Region Forest Research Report, 7th American Forest Congress*;
 931 U.S. Department of Agriculture: Forest Service, Southern Research Station, Asheville,
 932 NC, USA, Feb. 1996; 22pp.

933

934 2. Stanturf, J.A.; Wade, D.D.; Waldrop, T.A.; Kennard, D.K.; Achtemeier, G.L. Fires in

- 935 southern forest landscapes. In *The Southern Forest Resource Assessment*; Wear, D.M.,
936 Greis, J., Eds.; Gen. Tech. Rep. SRS-53 U. S. Department of Agriculture: Forest Service,
937 Washington, DC, USA, 2002; pp. 607-630.
- 938
- 939 3. Wade, D.D.; Brock, B.L.; Brose, P.H.; and others. Fire in eastern ecosystems. In:
940 *Wildland fire in ecosystems: effects of fire on flora*, Gen. Tech. Rep. RMRS-42 . Brown,
941 J.K., Smith, J.K., Eds.; U.S. Department of Agriculture: Forest Service, Rocky Mountain
942 Research Station, Ogden, UT, USA, 2000; pp. 53-96. (Chapter 4. Vol. 2.)
- 943
- 944 4. Achtemeier, G.L. Effects of moisture released during forest burning on fog formation
945 and implications for visibility. *Journal of Applied Meteorology and Climatology* **2008** ,
946 47, 1287-1296.
- 947
- 948 5. Achtemeier, G.L. On the formation and persistence of superfog in woodland smoke.
949 *Meteorological Applications* **2009**, 16, 215-225.
- 950
- 951 6. Naeher, L.P.; Achtemeier, G.L.; Glitzenstein, J.S.; MacIntosh, D.; Streng, D.R. Real-
952 time and time-integrated PM_{2.5} and CO from prescribed burns in chipped and non-
953 chipped plots – Firefighter and community exposure and health implications. *Journal of*
954 *Exposure Science and Environmental Epidemiology* **2006**.
955 <http://www.nature.com/doi/10.1038/sj.jea.7500497>
- 956
- 957 7. Zheng, M.; Cass, G.R.; Schauer, J.J.; Edgerton, E.S. Source Apportionment of PM_{2.5}
958 in the Southeastern United States Using Solvent-Extractable Organic Compounds as
959 Tracers. *Environmental Science and Technology* **2002**, 36, 2361-2371.
- 960
- 961 8. Liu, Y.-Q.; Achtemeier, G.L.; Goodrick, S. Sensitivity of air quality simulation to
962 smoke plume rise. *Journal of Applied Remote Sensing* **2008**, 2, 021503; 12 pp.
963 (DOI:10.1117/1.2938723)
- 964
- 965 9. Liu, Y.-Q.; Goodrick, S.; Achtemeier, G.L.; Jackson, W.A.; Qu, J.J.; Wang, W.
966 Smoke incursions into urban areas: simulation of a Georgia prescribed burn.
967 *International Journal of Wildland Fire* **2009**, 18, 336–348. (DOI:10.1071/WF08082)
- 968
- 969 10. Liu, Y.-Q.; Achtemeier, G.L.; Goodrick, S.; Jackson, W.A. Important parameters for
970 smoke plume rise simulation with Daysmoke. *Atmospheric Pollution Research* **2010**, 1,
971 250-259.
- 972
- 973 11. Odman, M.T.; Khan, M.N.; McRae, D.S. Adaptive grids in air pollution modeling:
974 Towards and operational model. In *Air Pollution Modeling and its Application XIV*, 1st
975 ed.; Gryning, S.E., Schiermeier, F.A., Eds.; Kluwer Academic/ Plenum Publishers: New
976 York, New York, USA, 2001; pp. 541-549.
- 977
- 978 12. Odman, M.T.; Khan, M.N.; Srivastava, R.K.; McRae, D.S. Initial application of the
979 adaptive grid air pollution model. In *Air Pollution Modeling and its Application XV*, 1st
980 ed.; Borrego, C., Schayes, G., Eds.; Kluwer Academic/ Plenum Publishers: New York,

- 981 New York, USA, 2002; pp. 319-328.
982
- 983 13. Lee, S.; Russell, A.G.; Baumann, K. Source apportionment of fine particulate matter
984 in the southeastern United States. *Journal of Air and Waste Management Association*
985 **2007**, 57, 1123-1135.
986
- 987 14. Hu, Y. M.; Odman, T.; Chang, M.E.; Jackson, W.; Lee, S.; Edgerton, E.S.; Baumann,
988 K. Simulation of air quality impacts from prescribed fires on an urban area.
989 *Environmental Science and Technology* **2008**, 42, 3676–3682.
990
- 991 15. Byun, D.W.; Ching, J. *Science algorithms of the EPA Model-3 community multiscale*
992 *air quality (CMAQ) modeling system*; National Exposure Research Laboratory: Research
993 Triangle Park, NC, USA, 1999; 77 pp. (EPA/600/R-99/030.)
994
- 995 16. Byun, D.W.; Schere, K.L. Review of the governing equations, computational
996 algorithms, and other components of the Models-3 Community Multiscale Air Quality
997 (CMAQ) modeling system. *Applied Mechanics Reviews* **2006**, 59, 51-77.
998
- 999 17. Herzog, M.; Graf, H.-F.; Textor, C.; Oberhuber, J. M. The effect of phase changes of
1000 water on the development of volcanic plumes. *Journal of Volcanology and Geothermal*
1001 *Research* **1998**, 87, 55-74.
1002
- 1003 18. Oberhuber, J. M.; Herzog, M.; Graf, H.-F.; Schwanke, K. Volcanic plume simulation
1004 on large scales. *Journal of Volcanology and Geothermal Research* **1998**, 87, 29-53.
1005
- 1006 19. Trentmann, J.; Andreae, M.O.; Graf, H.-F.; Hobbs, P.V.; Ottmar, R.D.; Trautmann, T.
1007 Simulation of a biomass-burning plume: comparison of model results with observations.
1008 *Journal of Geophysical Research* **2002**, 107, No. D2, 5-1 – 5-15.
1009
- 1010 20. Garcia-Menendez, F.; Yano, A.; Hu, Y.; Odman, M. T. An adaptive grid version of
1011 CMAQ for improving the resolution of plumes. *Atmospheric Pollution Research* **2010**, 1,
1012 239-249. (DOI: 10.5094/APR.2010.031).
1013
- 1014 21. Grell, G.A.; Peckham, S.E.; Schmitz, R.; McKeen, S.A.; Wilczak, J.; Eder, B. Fully
1015 coupled online chemistry within the WRF model. *Atmospheric Environment* **2005**, 39,
1016 6957-6975.
1017
- 1018 22. Lavdas, L.G. *Program VSMOKE–users manual*. USDA Forest Service General
1019 Technical Report SRS-6; U. S. Department of Agriculture: Forest Service, Southern
1020 Region, Asheville, NC, USA, 1996; 147 pp.
1021
- 1022 23. Goodrick, S.L.; Brenner, J. Florida’s Fire management information system. In
1023 *Proceedings of the Joint Fire Science Conference and Workshop, June 15-17, 1999*;
1024 University of Idaho Press: Boise, ID, USA, 1999; Vol. 1: 3-12. Available online at
1025 <http://jfsp.nifc.gov/conferenceproc/Goodricketal.pdf>
1026

- 1027 24. Brenner, J.; Goodrick, S.L. Florida's Fire Management Information System. In
1028 *Proceedings of EastFire Conference*; George Mason University: Fairfax, VA, USA; May
1029 2005; 4 pp.
- 1030
- 1031 25. Draxler, R.R.; Hess, G.D. *Description of the Hysplit_4 modeling system*; NOAA
1032 Technical Memorandum ERL ARL-224; Washington, DC, USA, December 1997; 24 pp.
1033
- 1034 26. Achtemeier, G.L. Predicting dispersion and deposition of ash from burning cane.
1035 *Sugar Cane* **1998**, 1, 17-22.
- 1036
- 1037 27. Achtemeier, G.L.; Adkins, C.W. Ash and smoke plumes produced from burning
1038 sugar cane. *Sugar Cane* **1997**, 2, 16-21.
- 1039
- 1040 28. Hess, S.L. *Introduction to Theoretical Meteorology*; Henry Holt & Co.: New York,
1041 NY, USA, 1959; 362 pp.
- 1042
- 1043 29. Briggs, G.A. Plume Rise Predictions. In *Lectures on Air Pollution and Environmental*
1044 *Impact Analyses*; American Meteorological Society: Boston, MA, USA, 1975; pp. 72-73.
1045
- 1046 30. Cukier, R.I.; Fortuin, C.M.; Shuler, K.E.; Petschek, A.G.; Schaibly, J.H. Study of the
1047 sensitivity of coupled reaction systems to uncertainties in rate coefficients. *I. Theory*
1048 *Journal of Chemical Physics* **1973**, 59, 3873-3878.
- 1049
- 1050 31. Deeming, J.E.; Lawrence, J.W.; Fosberg, M.A.; Furman, R.W.; Schroeder, M.J.
1051 *National fire danger rating system*; Rocky Mountain Forest and Range Experiment
1052 Station Research Paper RM—84; U. S. Department of Agriculture: Forest Service, Fort
1053 Collins, CO, USA, 1972; 165 pp.
- 1054
- 1055 32. Wade, D.D.; Lunsford, J.D. *A Guide for Prescribed Fire in Southern Forests*. U. S.
1056 Department of Agriculture: Forest Service, Southern Region, Asheville, NC, USA,
1057 February 1989. (Technical Publication R8-TP 11)
- 1058
- 1059 33. O'Neill, S.M.; Ferguson, S.A.; Peterson, J.; Wilson, R. The BlueSky Smoke Modeling
1060 Framework. In *Proceedings of the 5th Symposium on Fire and Forest Meteorology*;
1061 American Meteorological Society: Orlando, FL, USA, November 2003.
- 1062
- 1063 34. Ottmar, R.D.; Anderson, G.K.; DeHerrera, P.J.; Reinhardt, T.E. *Consume Version*
1064 *2.1 User's Guide*; U.S. Department of Agriculture: Forest Service, Pacific Northwest
1065 Research Station, Portland, OR, USA, 1999.
1066 (http://www.fs.fed.us/pnw/fera/products/consume/CONSUME21_USER_GUIDE.DOC)
1067
- 1068 35. Hao, W.M.; Personal communication; 2002.
- 1069
- 1070 36. Sandberg, D.V.; Peterson, J. A source strength model for prescribed fire in coniferous
1071 logging slash. Paper presented at 1984 annual meeting of the Air Pollution Control
1072 Association, Pacific Northwest section, Portland, OR, USA, 1984.

- 1073
1074 37. Andrews, P.L.; Bevins, C.D.; Seli, R.C. *BehavePlus fire modeling system, version*
1075 *3.0: User's Guide*. Gen. Tech. Rep. RMRS-GTR-106WWW Revised. U.S. Department of
1076 Agriculture: Forest Service, Rocky Mountain Research Station, Ogden, UT, USA, 2005;
1077 144 pp.
1078
- 1079 38. Byram, G.M. Combustion of forest fuels. In *Forest Fire control and Use*; Davis,
1080 K.P., Ed.; McGraw Hill: New York, NY, USA; pp. 155-182.
1081
- 1082 38. Mercer, G.N.; Weber, R.O. *Fire Plumes in Forest Fires: Behavioral and Ecological*
1083 *Effects*; Johnson, E.A., Miyanishi, K., Eds.; Academic Press: New York, New York,
1084 USA, 2001; pp. 225-256.
1085
- 1086 39. Jenkins, M.A.; Clark, T.; Coen, J. Coupling atmospheric and fire models. In *Forest*
1087 *Fires: Behavior and Ecological Effects*. Johnson, E.A., Miyanishi, K., Eds.; Academic
1088 Press: San Diego, CA, USA, 2001; pp.258-301.
1089
- 1090 40. Clements, C.B.; Zhong, S.; Goodrick, S.; Li, J.; Potter, B.E.; Bian, X.; Heilman,
1091 W.E.; Charney, J.J.; Perna, R.; Jang, M.; Lee, M.; Patel, M.; Street, S.; Aumann, G.
1092 Observing the dynamics of wildland grass fires: FireFlux – a field validation experiment.
1093 *Bulletin of American Meteorological Society* **2007**, 88, 1369-1382.
1094
- 1095 41. Cunningham, P.; Goodrick, S.L.; Hussaini, M.Y.; Linn, R.R. Coherent vertical
1096 structures in numerical simulations of buoyant plumes from wildland fires. *International*
1097 *Journal of Wildland Fire* **2005**, 14, 61-75.
1098
- 1099 42. Cunningham, P.; Goodrick, S.L. High-resolution numerical models for smoke
1100 transport in plumes from wildland fires. In *Remote Sensing and Modeling Applications to*
1101 *Wildland Fires*; Qu, J.J., Riebau, A., Yang, R., Sommers, W., Eds.; Dordrecht: Springer
1102 Publishing: New York, NY, USA, 2011; pp. 74-88. [in press].
1103
- 1104 43. Mills, M.T. Modeling the release and dispersion of toxic combustion products from
1105 pool fires. In *Proceedings International Conference on Vapor Cloud Modeling*;
1106 Cambridge, MA, USA, 1987.
1107
- 1108 44. Stern, A.C. *Air Pollution Volume I*; Academic Press: New York, New York, USA,
1109 1968; p. 51.
1110
- 1111 45. Fisher, B. E. A.; Metcalfe, E.; Vince, I.; Yates, A. Modelling plume rise and
1112 dispersion
1113 from pool fires. *Atmospheric Environment*, **2001**, 35, 2101-2110.
1114
- 1115 46. Liu, S. *Downwind real-time PM_{2.5} and CO monitoring during prescribed forest*
1116 *burns at Fort Benning, GA*. Master's Degree Thesis; University of Georgia: Athens, GA,
1117 USA, 2010; 104 pp.
1118

- 1119 47. Srivastava, R.K.; McRae, D.S.; Odman, M.T. An adaptive grid algorithm for air-
1120 quality modeling. *Journal of Computational Physics* **2000**, 165, 437-472.
1121
- 1122 48. Odman, M.T.; Hu, Y. A variable time-step algorithm for air quality models.
1123 *Atmospheric Pollution Research* **2010**, 1, 229-238. (DOI: 10.5094/APR.2010.030).
1124
- 1125 49. Anderson, G.; Sandberg, D.; Norheim, R. *Fire Emission Production Simulator*
1126 *(FEPS) User's Guide Version 1.0*; U.S. Department of Agriculture: Forest Service,
1127 Washington, DC, USA, 2004; 97 pp.
1128
- 1129 50. CEP, *Sparse Matrix Operator Kernel Emissions Modeling System (SMOKE) User*
1130 *Manual*; Carolina Environmental Program: The University of North Carolina at Chapel
1131 Hill, Chapel Hill, NC, USA, 2003.
1132
- 1133 51. MACTEC. *Documentation of the Revised 2002 Base Year, Revised 2018, and Initial*
1134 *2009 Emission Inventories for VISTAS*. Visibility Improvement State and Tribal
1135 Association of the Southeast (VISTAS) Ed.: Ashville, NC, USA, 2005.
1136
- 1137 52. Michalakes, J.; Dudhia, J.; Gill, D.; Henderson, T.; Klemp, J.; Skamarock, W.; Wang,
1138 W. The Weather Research and Forecast Model: Software Architecture and Performance.
1139 *In Proceedings of the Eleventh ECMWF Workshop on the Use of High Performance*
1140 *Computing in Meteorology*; Zwiefelhofer, W., Mozdzyński, G., Eds.; World Scientific:
1141 Singapore, 2005; pp. 156-168.